INDC(KOR)-006
Distr. NC

INDC International Nuclear Data Committee

Proceedings of the

Ninth AASPP Workshop on Asian Nuclear Reaction Database Development

The K Hotel, Gyeongju, Republic of Korea

12 – 15 November 2018

Edited by

Sung Chul Yang
Nuclear Data Center, Korea Atomic Energy Research Institute
Daejeon, Republic of Korea

and

Naohiko Otuka
Nuclear Data Section, International Atomic Energy Agency, Vienna, Austria

January 2019

IAEA Nuclear Data Section, Vienna International Centre, A-1400 Vienna, Austria

Selected INDC documents may be downloaded in electronic form from
http://www-nds.iaea.org/publications/
or sent as an e-mail attachment.
Requests for hardcopy or e-mail transmittal should be directed to
nds.contact-point@iaea.org
or to:

Nuclear Data Section
International Atomic Energy Agency
Vienna International Centre
PO Box 100
A-1400 Vienna
Austria

Produced by the IAEA in Austria
January 2019

INDC (KOR)-006
Distr. NC

Proceedings of the

Ninth AASPP Workshop on Asian Nuclear Reaction Database Development

The K Hotel, Gyeongju, Republic of Korea

12 – 15 November 2018

Edited by

Sung Chul Yang
Nuclear Data Center, Korea Atomic Energy Research Institute
Daejeon, Republic of Korea

and

Naohiko Otuka
Nuclear Data Section, International Atomic Energy Agency, Vienna, Austria

January 2019

Abstract

The 9th Workshop on Asian Nuclear Reaction Database Development was held from 12-15 November 2018 at the K Hotel in Gyeongju. This 9th workshop followed the workshops in Sapporo (Japan, 2010), Beijing (China, 2011), Pohang (Korea, 2012), Almaty (Kazakhstan, 2013), Mumbai (India, 2014), Sapporo (Japan, 2015), Beijing (China, 2016) and Ulaanbaatar (Mongolia, 2017). The workshop was organized by Nuclear Data Center, Korea Atomic Energy Research Institute in collaboration with the Asian Centres of the International Network of Nuclear Reaction Data Centres and supported by International Atomic Energy Agency. The topics of the workshop were sharing information on activities of the nuclear data centres, EXFOR compilation, data evaluation, computational simulations, software training and other related topics. The participants were attended from China, India, Japan, Kazakhstan, Korea, Mongolia, Vietnam and the IAEA. In the workshop, 24 presentations were presented and summarized in these proceedings.

Table of Contents

Agenda ··· 7

Compilation and dissemination of fission product yields ··· 11

Activity of nuclear reaction data in JCPRG ··· 15

Status of EXFOR activity in India and evaluation of neutron induced cross section ·· 18

EXFOR compilation at CNDC ··· 22

The systematics of thermal neutron fission cross sections ··· 27

EXFOR compilation and nuclear data measurement at KAERI/NDC ··· 33

Evaluation of photonuclear cross sections at KAERI ··· 36

Mass yield distribution in the ^{232}Th(n,f) reaction based on the ^{9}Be(p,n) reaction ··· 38

Study of nuclear reaction ^{141}Pr(γ,2n)^{139}Pr and ^{141}Pr(γ,pn)^{139}Ce induced with bremsstrahlung end-point energy in the range 50 – 70 MeV ··· 45

KAERI neutron time-of-flight (nTOF) facility – introduction and current status ··· 51

The first unbound states of mirror ^{9}B and ^{9}Be nuclei in the complex scaling method · 52

Refraction effects in the α and ^{3}He scattering on light nuclei at energies about 50 MeV ··· 57

Analysis of the ^{16}O(p,pn)^{15}O reaction using the CDCC method ··· 61

Development of a semi-empirical model for calculation of fission product yields ··· 65

Systematic study on charged-particle-induced reactions for medical radioisotope production ··· 68

Proton induced reaction cross sections of ^{nat}W with proton beam of 45 MeV ··· 71

Measurements of cross section for the theranostic radionuclide ^{67}Cu ··· 72

Visualization of fission product yield by NDPlot ··· 73

List of participants ··· 77

Agenda

Date	Time	Topics	Speaker
Nov. 12 (Mon)	10:00~18:00	EXFOR session	
Nov. 13 (Tue)	10:00~12:00	EXFOR session (cont.)	
	12:00~13:00	Lunch	
	13:00~13:50	Registration	
	13:50~14:00	Opening address	Y.O. Lee (KAERI)
	14:00~14:20	Compilation and dissemination of fission product yields	N. Otsuka (IAEA)
	14:20~14:40	Activity of nuclear reaction data in JCPRG	D. Ichinkhorloo (JCPRG)
	14:40~15:00	Status of EXFOR activity in India and evaluation of neutron induced cross section	V. Devi (IET)
	15:00~15:20	EXFOR compilation at CNDC and systematics of thermal neutron fission cross sections	J. Wang (CIAE)
	15:20~15:40	EXFOR compilation and nuclear data measurement at KAERI/NDC	S.C. Yang (KAERI)
	15:40~16:00	Coffee break	
	16:00~16:20	Evaluation of photonuclear cross sections at KAERI	Y.S. Cho (KAERI)
	16:20~16:40	Mass yield distribution in the ^{232}Th(n,f) reaction based on the ^{9}Be(p,n) reaction	H. Naik (BARC)
	16:40~17:00	Study of nuclear reaction ^{141}Pr(γ,2n)^{139}Pr and ^{141}Pr(γ,pn)^{139}Ce induced with bremsstrahlung end-point energy in the range 50 – 70 MeV	Nguyen Van Do (VAST)
	17:00~17:20	KAERI neutron time-of-flight (nTOF) facility - introduction and current status	J.W. Kim (KAERI)
	17:20~17:40	Development of 9 MeV electron accelerating tube for radiotherapy machine	M.W. Lee (DIRAMS)

	18:00~20:00	Welcome dinner	
Nov. 14 (Wed)	10:00~10:20	The first unbound states of mirror ^{9}B and ^{9}Be nuclei in the complex scaling method	M. Odsuren (NUM)
	10:20~10:40	Refraction effects in the a and ^{3}He scattering on light nuclei at energies about 50 MeV	T. Zholdybayev (INP)
	10:40~11:00	Analysis of the $^{16}O(p,pn)^{15}O$ reaction using the CDCC method	D. Ichinkhorloo (JCPRG)
	11:00~11:20	Coffee break	
	11:20~11:40	The status of nuclear data measurement in KNU	G.N. Kim (KNU)
	11:40~12:00	Neutron Data Production System	S.W. Hong (SKKU)
	12:00~12:20	Development of a semi-empirical model for calculation of fission product yields	J.H. Lee (KAERI, SKKU)
	12:20~14:00	Lunch	
	14:00~14:20	Systematic study on charged-particle induced reaction for medical radioisotopes production	M. Aikawa (Hokkaido Univ.)
	14:20~14:40	Proton induced reaction cross section of ^{nat}W with proton beam of 45 MeV	Nguyen Thi Hien (KNU)
	14:40~15:00	Measurements of cross-section for the theranostic radionuclide ^{67}Cu	J.K. Park (KAERI)
	15:00~15:20	Measurement of neutron capture yield and average capture cross section of Dysprosium isotopes at J-PARC	J.E. Lee (DAU)
	15:20~15:40	Coffee break	
	15:40~16:00	Laser spectroscopy and atomic structure calculations for nuclear properties	D.H. Kwon (KAERI)
	16:00~16:20	Theoretical study on the production of new neutron-rich isotopes in multi-nucleon transfer reactions	M.H. Mun (KISTI)
	16:20~16:40	Validation of thermal neutron scattering cross sections for heavy water based on molecular dynamics simulation	H.L. Hyun (KAERI)

	16:40~17:00	Visualization of fission product yield by NDPlot	Y. Jin (CIAE)
	18:00~20:00	Dinner	

Nov. 15 (Thu)	10:00~10:30	Closing session	
	10:30~12:00	Facility tour: proton linear accelerator (KOMAC)	
	12:00~14:00	Lunch	
	14:00~17:00	Sightseeing in Gyeong-ju	

Compilation and Dissemination of Fission Product Yields

N. Otuka, S. Okumura, T. Fukuda

Nuclear Data Section, International Atomic Energy Agency, A-1400 Vienna, Austria

The neutron-induced fission product yield is a key parameter to describe various phenomena in nuclear sciences (*e.g.*, nuclear fission physics, nuclear synthesis) and applications (*e.g.*, reactor operation, spent fuel processing, waste managements). Evaluations performed in USA by Meek, Rider and England [1-3] and in UK by Crouch, James, Mills et al. [4-6] have been widely known in the nuclear data community, and their latest evaluated data are available in the ENDF-B and JEFF libraries, respectively.

Evaluation of fission product yields heavily relies on the experimental data, and therefore preparation of the experimental fission product yields is the important step of evaluation at the beginning. When the Four Centres (NNCSC, CCDN, NDS, CJD) started exchange of neutron-induced reaction data in 1970s, however, they did not try to make EXFOR complete for the fission product yield. They considered that most of the existing data were summarized in published review articles, and concluded in 1972 that compilation must be done with high priority for those not covered in such review articles [7]. They also confirmed in 1975 that none of them have the manpower to devote to the fission product yield yet [8]. Under this situation, the abovementioned USA and UK evaluation groups developed their own experimental databases, which were published along with their evaluation results.

For the UK compilation, CCND developed a program to convert Crouch's experimental database ("Crouch Library") to NEUDADA in 1977 [9]. CCND also compared the fission product yield data coverage in the Crouch Library and EXFOR in 1980. They concluded that only 9% of the references in the Crouch Library was compiled in EXFOR [10], but without further attempt to fill the gap systematically. For the USA compilation, NNDC was asked to convert it into EXFOR in the 1987 Studsvik meeting [11]. V. McLane (NNDC) performed its automatic conversion to quasi-EXFOR entries, which were further upgraded by NDS, CNDC etc. Such EXFOR entries are currently seen with a status code RIDER, and sometimes with NCHKD (original reference not checked). The UK evaluation was benefitted from this systematic conversion of the USA compilation to EXFOR when the UKFY2 library (12958 measurements) was upgraded to UKFY3 library (14710 measurements) [12].

There was significant developments in experimental and theoretical studies of the fission product yield since the IAEA CPRs on “Compilation and evaluation of fission yield nuclear data” (1991-1996) [13] and “Fission product yield for the transmutation of minor actinide nuclear waste” (1997-2002) [14], and an IAEA Technical Meeting on “Fission product yields: Current status and perspectives” was held in 2016 in Vienna to discuss progress in the field of the fission product yield [15]. This meeting concluded that it maybe timely to investigate EXFOR and check the completeness with respect to the compilation performed in the IAEA CRPs.

Under this situation, we started checking of EXFOR and CINDA against the UK and USA fission product yield evaluation reports [3,6]. This assessment has been done by the following three steps:

1. Conversion of the reference information of each article cited in the UK and USA evaluation reports to the EXFOR/CINDA code string (e.g., Nucl. Data Sheets **120**(2014)272 to J,NDS,120,272,2014);
2. Search EXFOR entries including the reference code string;
3. Search CINDA records including the reference code string,

for ~650 articles cited in the UK evaluation and ~620 articles cited in the USA evaluation.

Table 1 shows an example of the assessment summary table. In this example, the second reference was found in EXFOR and it was listed with its EXFOR entry number. The first and third references were found only in CINDA, and therefore the “0” is given as a dummy EXFOR entry number with the laboratory codes found in CINDA. Our preliminary result for the UK compilation shows that about 65% of the articles cited in UK compilation are also compiled in EXFOR. We plan to finish this assessment by the end of March 2019, and to assign articles to data centres in the NRDC 2019 meeting (9-12 April 2019, Vienna) for their compilation.

Table 1. Example of the assessment summary table.

Author	**Reference**	**EXFOR**	**Lab.**	**Remarks**
K.A.Petrzhak+	R,AEC-TR-4696,1961	0	4RUSRI	English translation of B,NEJTRONFIZ,,217,1961
B.P.Bayhurst	R,TID-5787,1957	13432	1USALAS	
H.V.Weiss+	R,USNRDL-TR-943,1965	0	1USANRD	Superseded

The aforementioned 2016 Vienna Technical Meeting [15] also expressed that dissemination of the fission product yield is another important point to be taken seriously by data centres. For example, Liu Tingjin pointed out that the retrieval and processing of fission yield data evaluation are quite complicated in the following aspects [16]:

1. The fission product nuclides in EXFOR can be a variable of the data table under the heading ELEMENT and MASS.
2. There are ratios or even double ratios (R-value) of the fission product yields in EXFOR.
3. Some parameters such as standard yield and gamma intensities should be readable in EXFOR for corrections of the published data.

A part of these problems could be solved by providing all data in a unified format, and the Computational Format (C4 [17]) is such a candidate. Possible extension of the C4 format to the fission product yield related quantities defined in the EXFOR/CINDA dictionary is summarized in **Table 2**.

Table 2. C4 format for fission product yield related quantities (proposal).

EXFOR REACTION code	Explanation	MT	Field 5	Field 6	Field 7	Field 8
(*,F)ELEM/MASS,IND,FY	Independent FPY	454		Prod. ZA		
((*,F)ELEM/MASS,IND,FY)/ ((*,F)MASS,CHN,FY)	Fractional independent FPY	1454		Prod. ZA		
(*,F)ELEM/MASS,CUM,FY	Cumulative FPY	459		Prod. ZA		
((*,F)ELEM/MASS,CUM,FY)/ ((*,F)MASS,CHN,FY)	Fractional cumulative FPY	1459		Prod. ZA		
(((*,F)ELEM/MASS,CUM,FY)/ ((*,F)CUM,FY))// (((*,F)ELEM/MASS,CUM,FY)/ ((*,F)CUM,FY)))	Cumulative FPY R-value	2459	Ref. proj. energy	Prod. ZA	Ref. targ. ZA	Ref. prod. ZA
(*,F)MASS,CHN,FY	Chain FPY	801		Prod. A		

Ref.: Reference reaction. Proj.: Projectile. Prod.: Product. Targ.: Target.

Fields 1 and 2 are always for the projectile energy and its uncertainty.

Fields 3 and 4 are always for the quantity measured and its uncertainty.

References

[1] M.E. Meek, B.F. Rider, NEDO-12154 (1972), NEDO-12154-1 (1974), NEDO-12154-2E (1978).

[2] B.F. Rider, NEDO-12154-3C (1981).

[3] T.R. England, B.F. Rider, LA-UR-94-3106 (1994).

[4] E.A.C. Crouch, At. Data Nucl. Data Tables **19** (1977) 419.

[5] M.F. James, R.W. Mills, D.R. Weaver, Prog. Nucl. Energy **26** (1991) 1; AEA-TRS-1018 Part II, 1991.

[6] R.W. Mills, "Fission product yield evaluation", PhD thesis submitted to University of Birmingham (1995).

[7] A. Calamand, J.R. Lemley, Report INDC(NDS)-51, International Atomic Energy Agency (1973).

[8] G. Thompson, N. Holden, Report INDC(NDS)-68, International Atomic Energy Agency (1975).

[9] H.D. Lemmel, Report INDC(NDS)-90, International Atomic Energy Agency (1977); H. Derrien, A. Schett, Memo 4C-2/89, Neutron Data Compilation Centre (1977).

[10] P.D. Johnston, Memo 4C-2/115, Neutron Data Compilation Centre (1980).

[11] M. Lammer, Report INDC(NDS)-208, International Atomic Energy Agency (1988).

[12] R.W. Mills, Report IAEA-TECDOC-1168 Section 7.2, International Atomic Energy Agency (2000).

[13] M. Lammer et al., Report IAEA-TECDOC-1168, International Atomic Energy Agency (2000).

[14] M. Lammer et al., Report STI/PUB/1286, International Atomic Energy Agency (2008).

[15] P. Dimitriou, F.-J. Hambsch, S. Pomp, INDC(NDS)-713, International Atomic Energy Agency (2016).

[16] Liu Tingjin, Report INDC(CPR)-44, p103, International Atomic Energy Agency (1998).

[17] D.E. Cullent, A. Trkov, Report IAEA-NDS-80 Rev. 1, International Atomic Energy Agency (2001).

Activity of Nuclear Reaction Data in JCPRG

D.Ichinkhorloo[1], M.Aikawa[2], M.Kimura[1,2], S.Imai[3], S.Jagjit[1], N.Otsuka[4,5] and T.Tada[6]

[1] *Nuclear Reaction Data Centre, Faculty of Science, Hokkaido University, Sapporo 060-8610, Japan*

[2]*Faculty of Science, Hokkaido University, Sapporo 060-8610, Japan*

[3]*Institute for the Advancement of Higher Education, Sapporo 060-0817, Japan*

[4]*RIKEN Nishina Center, 2-1, Hirosawa, Wako, Saitama 351-0198, Japan*

[5]*Nuclear Data Section, IAEA, Wein A-1400, Austria*

[6]*Graduate School of Science, Hokkaido University, Sapporo 060-8610, Japan*

1. Introduction

Nuclear reaction data such as the data of cross sections, radiations emitted from radioactive isotopes, level properties of isotopes are used widely in different fields. Nuclear data play a key role in understanding the nature of nuclear structures and nuclear reactions. At the same time, as the fundamental input to various codes for nuclear applications, they are also very important in medical radiotherapy, shielding and radiation protection, and some related engineering works. Therefore, it is of great significance to build a nuclear database for providing nuclear data service in various fields. Experimental data are found in the EXFOR [1] database, which is maintained by the International Atomic Energy Agency (IAEA) [2] and the International Network of Nuclear Reaction Data Centres (NRDC). The NRDC collaborates in database compilation and related software development. One of the NRDC members is the Hokkaido University Nuclear Reaction Data Centre (JCPRG) [3]. Under collaboration with the NRDC network, experimental data published in scientific journals are continuously surveyed.

2. Nuclear reaction data activity

In JCPRG, we have developed mainly four contents which are compilation, application, experiment and evaluation.

The charged-particle and photon induced data obtained from the facilities in Japan should be compiled by JCPRG. It has contributed to about 10 percent of the data on charged-particle nuclear reactions in the EXFOR database. In the JCPRG, compiled nuclear reaction data in the NRDF (Nuclear Reaction Data File) and EXFOR formats are available through the online search system, respectively. We also have developed an editor to support correct compilation and to maintain the quality of the database. The editor is based on web, which is named HENDEL (Hyper Editor for Nuclear Data Exchange Libraries) [4]. HENDEL is the editing system of charged-particle nuclear reaction data by using web browsers which allows us to output easily the EXFOR and NRDF files simultaneously

In this year, we have transmitted 46 new and 17 revised entries to Nuclear Data Section in IAEA. All data are accessible by the entry numbers listed in Table 1.

Table 1. Transmitted entry numbers in 2018

TRANS	ENTRY New	ENTRY Rev.
E109	1	1
E110	0	5
E111	0	4
E112	5	7
E113	14	0
E114	6	0
E115	9	0
E116	4	0
E117	7	0
Total	**46**	**17**

During the compilation process, it is necessary to convert graphical data on papers into numerical data. In the past, an input device called ’digitizer’ was used for reading the numerical data from printed matters. The software GSYS [5] developed in JCPRG is openly available for reading the numerical data from image files. We also have developed new editor for compilation for EXFOR output. The developing editor called ForEX is represented in Java programing language for the operation-system independent software.

The members of the JCPRG perform the experiments to measure the production cross section of radio isotopes for nuclear medicine. Also we perform theoretical calculation for nuclear reaction and nuclear structure.

3. Summary

Nuclear reaction data compilation is important in widely different fields of nuclear physics. JCPRG is a nuclear data centre to compile data for charged particle and nucleus nuclear reaction given in Japan. We have also developed application, experiments and evaluation.

Reference

[1] http://www.jcprg.org/exfor.
[2] http://www-nds.iaea.org.
[3] http://www.jcprg.org.
[4] http://www.jcprg.org/hendel.
[5] http://www.jcprg.org/gsys.

Status of EXFOR Activity in India and Evaluation of Neutron Induced Cross-section

Vidya Devi

IET Bhaddal Ropar, Punjab-India

vidyathakur@yahoo.co.in

In India, EXFOR compilation on a regular basis has been started since 2006. EXFOR compilation in INDIA is the outcome of the initiative and efforts undertaken by Nuclear Data Physics Centre of India (NDPCI). Since the past few years, EXFOR compilation has also been done by Universities through funds given by NDPCI-BRNS. All EXFOR compilations were done under the supervision of NDS, IAEA (Previously with the help of Dr. O. Schwerer, Dr. S. Dunaeva and currently with Dr. N. Otsuka).

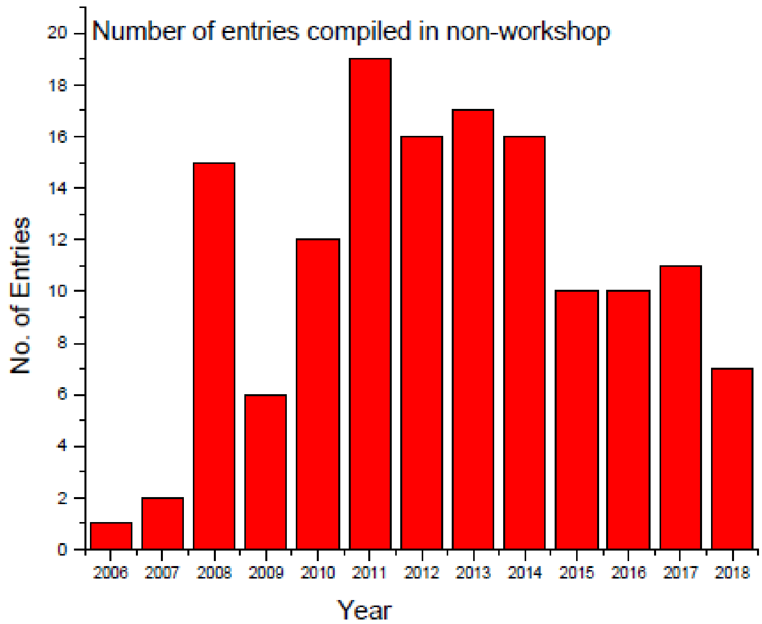

Fig. 1. Total number of entries for non-workshop or regular compilation activity since 2006.

1. Evaluation of neutron induced cross-section:

We need nuclear cross section data to explain various processes in development as well as research applications. The data of different experiments for a given reaction remain available in the EXFOR [1] database. But the data in general do not agree with

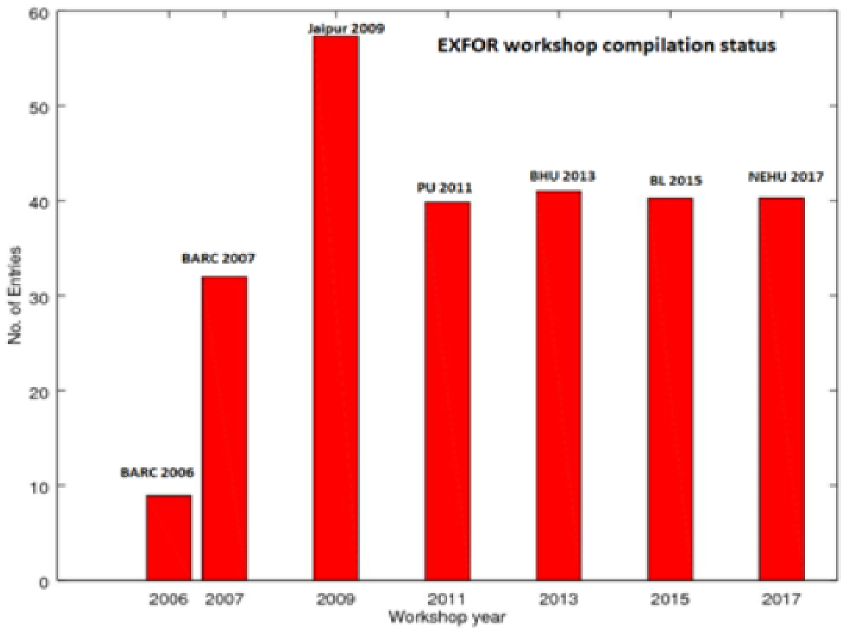

Fig. 2. Total number of entries for workshop since 2006.

each other and discrepancies do exist. There is a dire need of evaluation of data as various application and specialization rely on accurate data. Sodium metal has uses in Sodium-cooled Fast Reactor (SFR) as a coolant ^{23}Na is stable isotope of sodium and unlike water it absorbs less number of neutrons. In this work we are evaluating ^{23}Na isotope of Sodium metal by removing the errors or discrepancies in Na neutron induced cross section data for (n,2n) reaction and to give best fit.

In EXFOR there exist 20 sets of data of ^{23}Na for (n,2n) reaction channel. We only consider 11 sets out of 20 EXFOR sets. The EXFOR data sets without satisfactory monitor cross section information were discarded [2].

For evaluation procedure we first corrected data with reference to new standard monitor cross section for all data sets. The correction of cross section data has been carried out using ^{23}Na cross section as standard cross section in

$$\sigma_n = \frac{\sigma_{SN}}{\sigma_{SO}} \sigma_O$$

where σ_{SO} is the old standard cross section and σ_{SN} is the new standard cross section

^{23}Na(n,2n) cross section retrieved from ENDF/B-VIII.0. There were still large discrepancies present in the data. For construction of Covariance we used total as well as partial errors. Only common errors (e.g. efficiency of detector, branching fraction, thickness, monitor cross section) were used to construct partial errors.

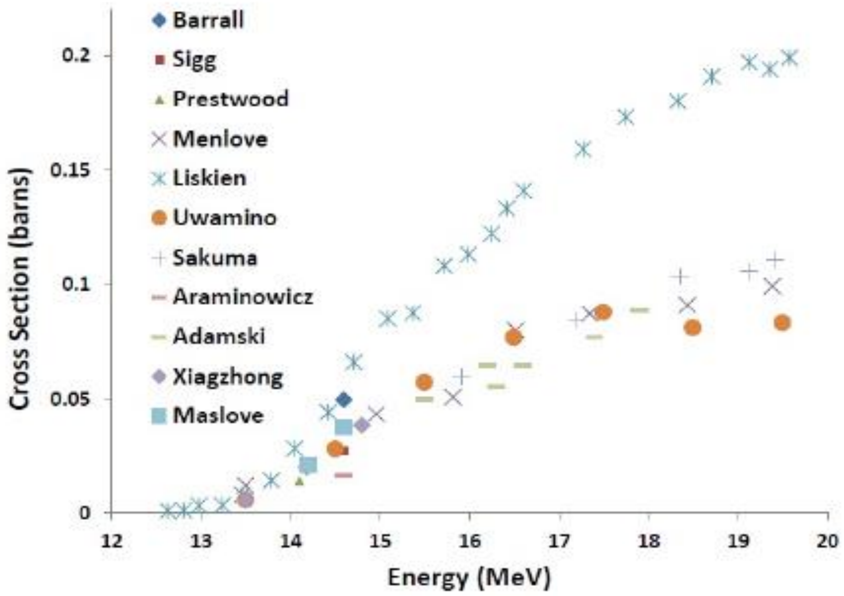

Fig. 3. Corrected cross section data retrieved from EXFOR.

Total errors will be used for diagonal entries of covariance matrix and partial errors contribute to non-diagonal entries. Correlation matrix was calculated from covariance matrix using equation

$$\langle Corr_{ij} \rangle = \frac{\langle Cov_{ij} \rangle}{\sqrt{Cov_{ii} Cov_{jj}}}$$

Cubic B-spline fitting procedure was used to fit normalized data sets. The considered data sets were contained 57 data points in the energy range below 20 MeV. Correlation matrices were used as an input in the spline code [3-4]. The evaluated data is represented as a solid curve in **Fig. 4(a)**, and comparison with other data libraries has been done in **Fig. 4(b)** [5].

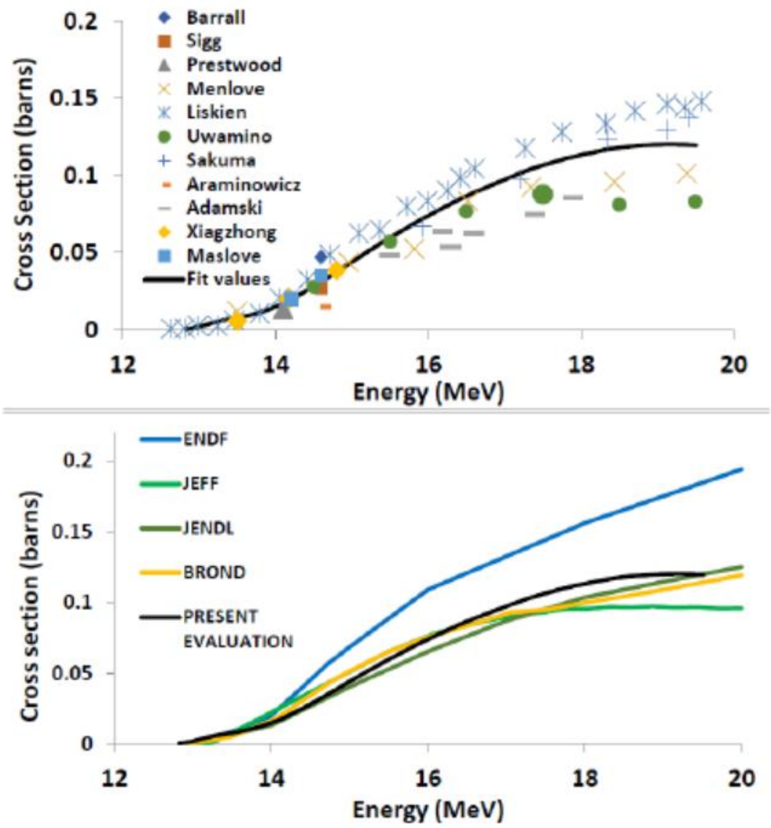

Fig. 4. (a) Normalized and B-Spline fitted value for cross section data; (b) Comparison of Evaluated data with other evaluation libraries.

2. Conclusion:

Special attention was paid to different sources of errors that are common to all data points and corrections are applied accordingly to remove these errors. The evaluated data is consistent with JENDL for low values and lie above JENDL for higher values. Evaluation of ^{23}Na(n,2n) is attempted in this work and it is found that cubic B-Spline gives better result as compared to the linear and quadratic B-Spline.

References

[1] https:www.nds.iaea.org/exfor/exfor.htm.

[2] J. Qian et al., Nucl. Sci. Eng. **171** (2012) 192.

[3] T. J. Liu and H. M. Zhou, Commun. Nucl. Data Prog. **11** (1994) 116.

[4] T. Lyche and K. Mørken “Spline Methods Drive” (2008).

[5] Carl de Boor, SIAM J. Numer. Anal., **14** (1977) 441.

EXFOR Compilation in CNDC

Jimin Wang, Xi Tao, Yongli Jin, Guochang Chen, Jing Qian, Lile Liu, Zhigang Ge

China Nuclear Data Center, China Institute of Atomic Energy, Beijing 102413, China

1. Introduction

The EXchange FORmat (EXFOR) experimental nuclear reaction database and the associated Web interface provide access to the wealth of low- and intermediate-energy nuclear reaction physics data [1]. The EXFOR library has become the most comprehensive compilation of experimental nuclear reaction data [2]. It contains cross sections and other nuclear reaction quantities induced by neutron, charged-particle and photon beams. Compilation is mandatory for all low and intermediate energy (≤1GeV) neutron and light charged-particle (A≤12) induced reaction data. Heavy-ion (A≥13) and photon induced reaction data are also compiled on a voluntary basis.

Currently, 13 nuclear data centers from the USA, OECD/Data Bank(France), IAEA/NDS (Austria), Russian Federation, China, Hungary, India, Japan, Kazakhstan, Korea, and Ukraine participate in the International Network of Nuclear Reaction Data Centers (NRDC) which has been organized under the auspices of the International Atomic Energy Agency to coordinate the collection, compilation, and dissemination of nuclear data on an international scale [3].

Since China joined IAEA in 1984 and China Nuclear Data Center (CNDC) joined NRDC in 1987, CNDC does its best for scanning Chinese journals, compiling EXFOR entries, developing softwares, providing nuclear data service in China and collaborating with NRDC. The experimental nuclear reaction data compiled by CNDC include the measurements were carried out by Chinese researcher, measured in China and published in Chinese journals.

2. Compilation

The first important step in data compilation is to scan the literature and identify articles reporting experimental data for EXFOR compilation. Currently, CNDC is respond more than 7 Chinese journals (**Table 1**). Then to communicate with the authors and ask for the original numerical data and relevant experimental information for maintaining good quality of the EXFOR library. Finally, to compile these information and data as EXFOR format.

In 1985, the first charged particle induced reaction for EXFOR entry S0001 was compiled by Prof. Youxiang Zhuang. Compilation of neutron induced reaction was started in 1989, and the first entry 32501was compiled by Prof. Qichang Liang. During 2004 and 2009, the compilation was taken charge by Prof. Hongwei Yu.

Table 1. Main Chinese journals of responsibility for CNDC

Journal Name	Former title	Abb.	Language	First issue
Chinese Physics C		CPH/C	English	2007
	High Energy Physics and Nuclear Physics	HEN	English	1987
	High Energy Physics and Nuclear Physics	PHE	Chinese	1977
Atomic Energy Science and Technology		CST	Chinese	1959
Journal of Nuclear and Radiochemistry		HFH	Chinese	1979
Nuclear Techniques		NTC	Chinese	1978
Nuclear Science and Techniques		CNST	English	1989
Chinese Physics Letters		CPL	English	1984
Acta Physica Sinica		ASI	English	1933
Proceedings, Journal of University, etc.				

In 2009, EXFOR group was set up to take charge of compilation in CNDC, and consists of 6 members now. The information such as the assigned entry No., articles in pdf, authors, publication date, delayed date, the compiler and the processing of compilation are regularly uploaded to the EXFOR compilation management Website (**Fig. 1**).

Since 2010, CNDC has compiled 216 EXFOR entries as shown in **Fig. 2**, which included 105 neutron and 111 charged particle entries, constitute about 65% of entries from China. After the NRDC meeting (1-4 May, 2018), 31 entries have been compiled up to now, which included 21 neutron and 10 charged particle or heavy-ion induced reactions.

Fig. 1. EXFOR compilation management website.

Since 2014, N.Otsuka from IAEA/NDS concentrates a week for compiling, checking and correcting with our group in CNDC every year. That is an efficiency way for EXFOR compilation work. In 2018, during our collaborations, we finalized more than 10 entries, scanned the earlier issues of “Atomic Energy Science and Technology” and identified the candidates of EXFOR compilation.

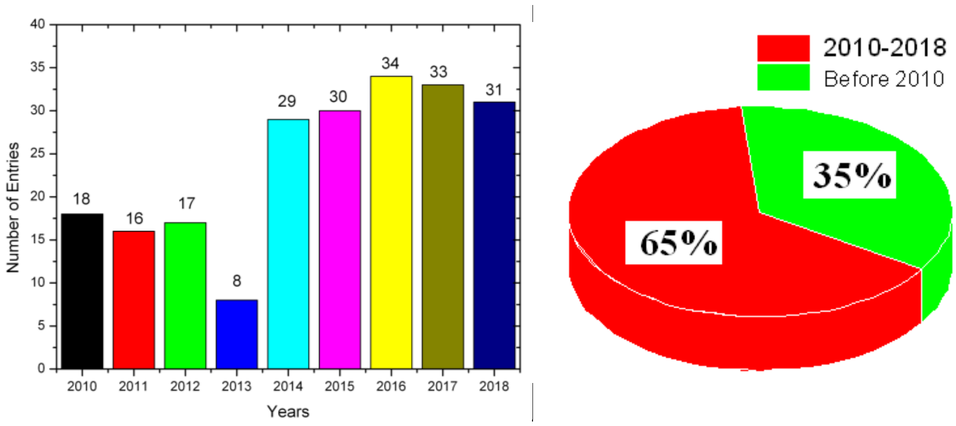

Fig. 2. Compiled EXFOR entries of each year and contribution of 2010-2018.

3. Development of software

For more than 30 years, CNDC makes great efforts to EXFOR compilation and development of relevant software. In 1993, the ERES code [4] was developed for

EXFOR compilation, but now it has been replaced by others.

Since 1997, CNDC devotes to develop software for digitization. The first version of Graph Digitizing System GDGraph [5] was released in 2000. The 2nd version of GDGraph was released in 2006, in which the code was re-written using Perl computer language. The versions of 3.0, 4.0, 5.0 and 5.1 were released in 2011, 2012, 2013 and 2016, respectively. The latest version will be released in 2019.

NDPlot [6] is an efficient plotting tool for nuclear data was developed by Dr. Yongli Jin in 2017 for upgrading code TT (TT is a window plotting tool and released in 2002, in Chinese). It is not only a plotting tool for nuclear data, but also integrated application software. The new features of NDPlot are introduced in this proceeding by Dr. Yongli Jin.

Fig. 3. The Database of Nuclear Physics.

4. Nuclear Data Service

CNDC provides the nuclear data service for institutes, universities or other requirements in China. CNDC joined the developing of Chinese basic database and established the Website of "The Database of Nuclear Physics" [7] (**Fig. 3**) including experimental data (EXFOR), evaluated data, nuclear structure and decay data, astrophysical data and nuclear data for medical applications, etc. Some software can be downloaded from the website, such as GDGraph, NDPlot, and so on.

CNDC also established the mirror site of IAEA-NDS in China, which Website is "www-nds.ciae.ac.cn". The database of this mirror site is updated with IAEA-NDS Website at the same time. Up to now, the contents of mirror site include EXFOR database and evaluation database, and the contents will be enriched in the future.

5. Conclusion

EXFOR is the major nuclear physics database for nuclear reactions. CNDC EXFOR group devotes to scan journals, collect numerical data and compile the measurements and its information which were carried out in China, measured by Chinese researchers or published in Chinese journals. In addition, CNDC does its best for developing softwares and providing nuclear data service in China. CNDC will continue to collaborate with NRDC and NRDC Asia on EXFOR compilation, software development, data evaluation, etc.

References

[1] V.V. Zerkin, B. Pritychenko, "The experimental nuclear reaction data (EXFOR): Extended computer database and Web retrieval system", Nucl. Inst. Meth. A **888** (2018) 31.

[2] N. Otsuka et al., "Towards a More Complete and Accurate Experimental Nuclear Reaction Data Library (EXFOR): International Collaboration Between Nuclear Reaction Data Centres (NRDC)", Nucl. Data Sheets **120** (2014) 272.

[3] Otto Schwerer (ed.), IAEA Report IAEA-NDS-207 (Rev.2015/08), IAEA, Vienna, Austria (2015).

[4] Li Shubing, Liang Qichang, Liu Tingjin, ERES A PC Program for Nuclear Data Compilation in EXFOR Format, IAEA-NDS-151, 1994.

[5] GDGraph 5.1 Manual, a tool for digitization of graph image, prepared by Jin Yongli and Chen Guochang, IAEA-NDS-216, 2016.

[6] http://www.nuclear.csdb.cn/ndplot/.

[7] http://www.nuclear.csdb.cn/.

The Systematics of Thermal Neutron Fission Cross Sections

Jimin Wang, Haicheng Wu, Xi Tao, Guochang Chen, Zhigang Ge

China Nuclear Data Center, China Institute of Atomic Energy, Beijing 102413, China

Based on the fission theory, the systematics formulae of thermal neutron fission cross sections have been established. On the basis of the recommended thermal neutron fission cross sections and the height of the fission barrier, the correlations between thermal neutron fission cross sections and the excitation energy of saddle point have been studied, the local parameters corresponding to Z have been obtained by fitting. Then, the systematics behaviors of these parameters with Z have been studied, the odd-even relations have been found. The results indicate that there are the correlations between thermal neutron fission cross sections and proton number.

1. Introduction

The thermal neutron fission cross sections of actinides are important for design of the nuclear installation, nuclear energy application and understanding of nuclear fission. However, the measured data are scarce and scattered for some nuclei. Generally, the systematics are convenient and reliable for prediction of the neutron induced reaction cross sections, compared to model theory calculations when experimental data are scarce.

Earlier works on systematics of thermal neutron fission cross sections of actinides were performed by H.Diamond et al. [1] and Gu Fuhua et al. [2]. The former was for the odd-odd nuclide, and the later have obtained the correlation between the fission cross sections and the mass number A, but the predicted cross sections were deviated because the experimental data have been used in the work are incomplete measured data of the thermal neutron fission cross sections.

New measurements have been performed with the development of the conditions and technology of experiment. In present work, the systematics formulae of thermal neutron fission cross sections of actinides have been established, the systematics behaviours of thermal neutron fission cross sections of actinides have been studied.

2. Formulae

Based on the fission theory [3], the fission cross sections can be written as

$$\sigma_f \approx \sigma_r \frac{\Gamma_f}{\Gamma} = \sigma_r \frac{\Gamma_f}{\Gamma_f + \Gamma_n}$$

Where, Γ is the total width, Γ_f is the fission width and Γ_n is the neutron width. On basis of the Hill-Wheeler formula, the Γ_f can be solved by the following

$$\Gamma_f(E) = \frac{1}{2\pi\rho(E)} \int_0^\infty \rho_f(E - V_f - \varepsilon) T(E) d\varepsilon$$

Where, ρ_f is the level density of the saddle point, E is the excited energy of compound nucleus, V_f is the height of single-humped fission barrier and $T(E)$ is the transmission coefficient of barrier.

$$T(E) = \left\{1 + \exp\left[-2\pi(E - V_f)/\hbar\omega\right]\right\}^{-1}$$

$E - V_f$ is the excitation energy of saddle point, and is the parameter for calculating the $T(E)$ and the fission width Γ_f. For the thermal neutron fission cross sections, the effective excited energy of compound nucleus is mainly from the neutron binding energy B_N and the pairing correction Δ, then the systematics formula of thermal neutron fission cross sections of actinides can be expressed approximately as

$$\ln\sigma_f = a\ln(B_N - \Delta - V_f + E_{sh}) + b$$

Where, a and b are the systematics parameters, E_{sh} is the energy shift factor (3 in this work), pairing correction Δ be expressed as

$$\begin{aligned} \Delta &= 12/A^{1/2} && even - even \\ &= 0 && odd \\ &= -12/A^{1/2} && odd - odd \end{aligned}$$

3. Data selection

The experimental data for thermal neutron fission cross sections were taken from EXFOR. For some nuclei, the evaluated data were used in this work and taken from BNL-325 [4], ENDF/B-VII.0 [5], CENDL-3.1 [6] and JENDL-4.0 [7]. There are 81 thermal neutron fission cross sections with the uncertainty have been recommended from ^{227}Th to ^{257}Fm.

Based on the CENDL-3.1, the work of Moller et al. [8], RIPL [9] and JENDL-4.0, the height of single-humped fission barrier for 81 nuclei from ^{227}Th to ^{257}Fm have been recommended.

4. Parameter correlations

Firstly, the thermal neutron fission cross sections have been studied on the different proton number. Then, on the basis of the fitted parameters, the correlations between the parameters and proton number can be expressed as simple functions.

$$\ln\sigma_f = b(Z)\times\ln(B_N - \Delta - V_f + 3) + a(Z)$$

$$a(Z)=\begin{cases}-2.03\times Z + 205.84 & odd\ \ Z\\ -0.34\times Z^2 + 63.95\times Z - 2984.37 & even\ Z\end{cases}$$

$$b(Z)=\begin{cases}2.99\times Z - 295.73 & odd\ \ Z\\ 0.43\times Z^2 - 79.14\times Z + 3676.12 & even\ Z\end{cases}$$

Table. 1 Local parameters of *a* and *b*.

element	***a***	***b***	$\sqrt{\chi^2}$
90-Th	6.30397	-3.78777	1.75764
91-Pa	22.0691	-24.1842	2.59399
92-U	9.52714	-7.2304	2.11196
93-Np	16.9183	-17.0798	1.4206
94-Pu	11.2275	-6.8399	1.63311
95-Am	13.1164	-10.6148	1.78953
96-Cm	8.74341	-4.90591	1.25538
97-Bk	7.60433	-2.8565	0.353026
98-Cf	4.50222	2.78259	1.85221
99-Es	6.45147	-1.34662	2.68868

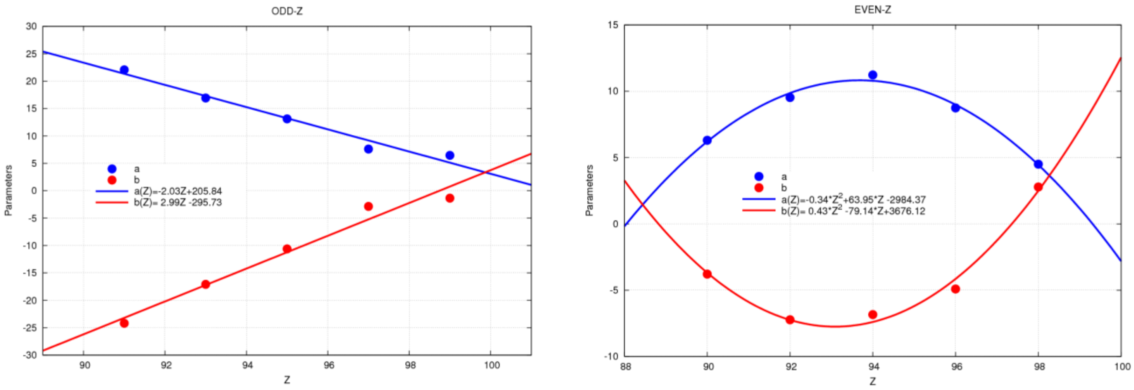

Fig.1. The correlations between local parameters and Z.

5. Results and discussion

Using the regional parameters, the thermal neutron fission cross sections of actinides have been calculated. The results are shown in **Figs. 2** through **6**, in which the black points are from experiment or evaluation, the blue square points are predicted values, the solid line is the results calculated from this systematics.

The results indicate that the C/E of the 28 nuclides or their reciprocal is less than 2. The C/E of the 52 nuclides or their reciprocal is less than 5. The C/E of the 22 nuclides or their reciprocal is larger than 10. The reason of deviation may be from fission barriers, recommended values and systematics formula. The improvement is expected to obtain in future.

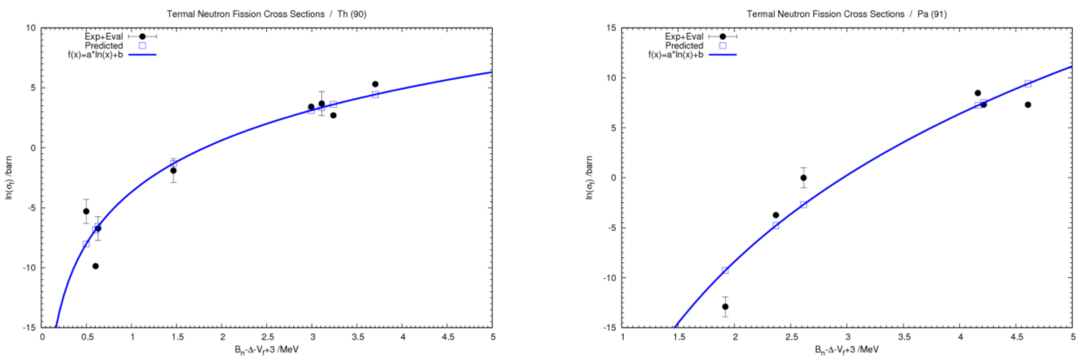

Fig.2. Comparison of predicted values with evaluated or measured for Th and Pa.

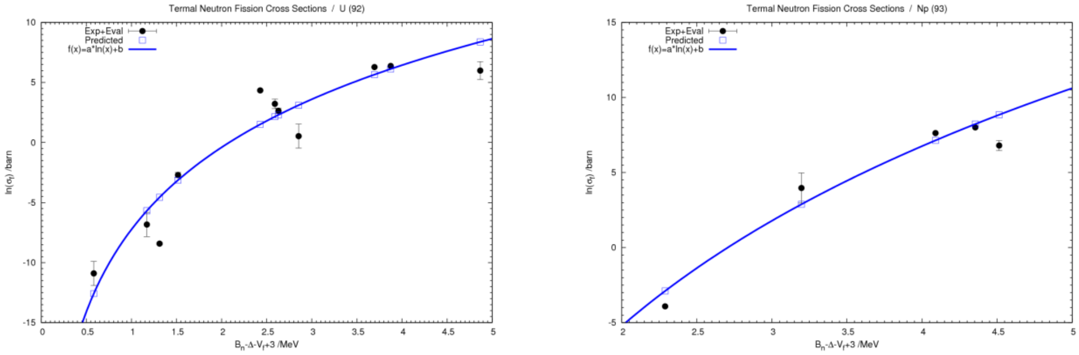

Fig.3. Comparison of predicted values with evaluated or measured for U and Np.

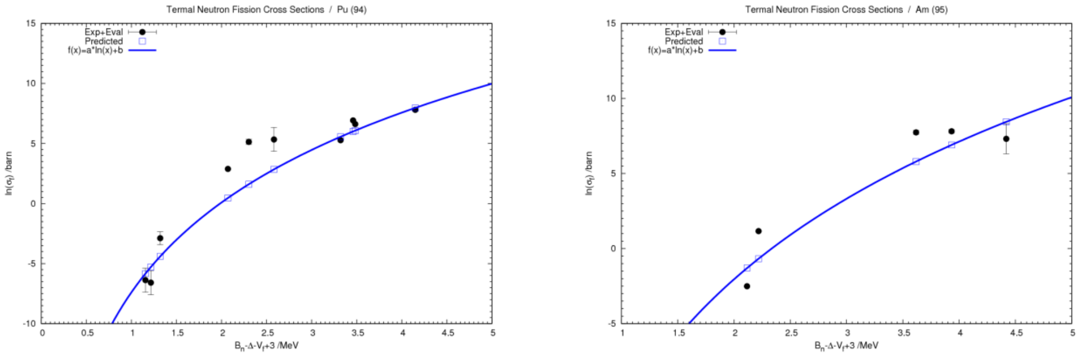

Fig.4. Comparison of predicted values with evaluated or measured for Pu and Am.

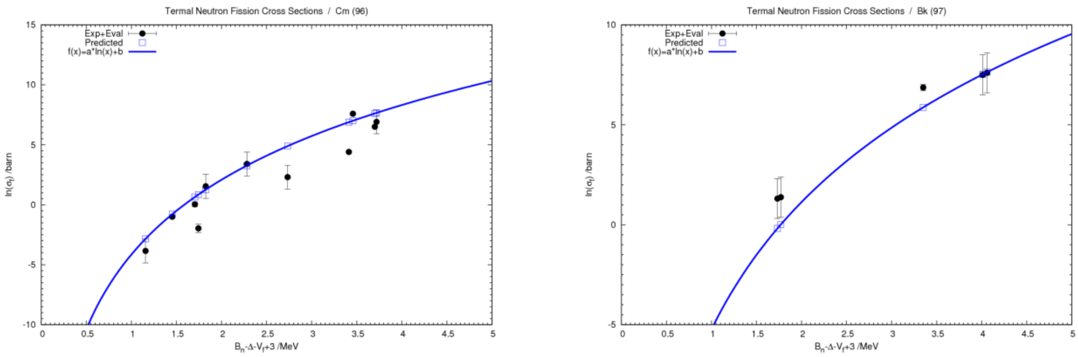

Fig.5. Comparison of predicted values with evaluated or measured for Cm and Bk.

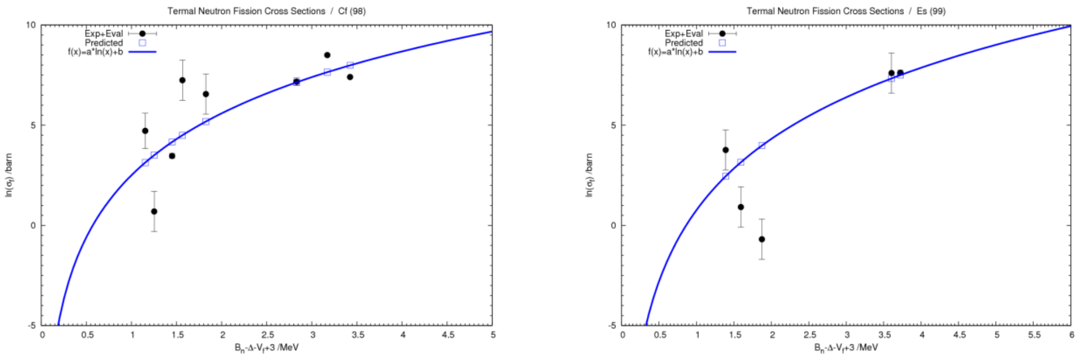

Fig.6. Comparison of predicted values with evaluated or measured for Cf and Es.

References

[1] H. Diamond et al., J. Inorg. Nucl. Chem. **30** (1968) 2553.

[2] Gu Fuhua, Liu Jicai, Some systematic characteristics of thermal neutron fission cross sections for actinides, Atom. Energy Sci. Technol. **39** (1985) 39 (in Chinese).

[3] Wang Shunuan, The theory of nuclear reaction, The Press of Atomic Energy, 2007 (in Chinese).

[4] S.F. Maghabghab, Atlas of neutron resonances, Elsevier Science, 2006.

[5] M.B. Chadwick, P. Oblozinsky, M. Herman et al., ENDF/B-VII.0: Next Generation Evaluated Nuclear Data Library for Nuclear Science and Technology, Nucl. Data Sheets **107** (2006) 2931.

[6] Ge Zhigang, Zhuang Youxiang, Liu Tingjin et al., The Updated Version of Chinese Evaluated Nuclear Data Library (CENDL-3.1), J. Korean Phys. Soc. **59** (2011) 1052.

[7] K. Shibata, O. Iwamoto, T. Nakagawa et al., JENDL-4.0: A New Library for Innovative Nuclear Energy Systems, J. Korean Phys. Soc. **59** (2011) 1046.

[8] Peter Moller, Arnold J Sierk, Akira Iwamoto, Five-Dimensional Fission-Barrier Calculations from ^{70}Se to ^{252}Cf, Phys. Rev. Lett. **92** (2004) 072501.

[9] R. Capote, M. Herman, P. Oblozinsky et al., RIPL – Reference Input Parameter Library for Calculation of Nuclear Reactions and Nuclear Data Evaluations, Nucl. Data Sheets **110** (2009) 3107.

EXFOR Compilation and Nuclear Data Measurement at KAERI/NDC

S.C. Yang, T.Y. Song, Y.O. Lee

Nuclear Data Center, Korea Atomic Energy Research Institute, Daejeon, Korea

KAERI/NDC has compiled domestic nuclear reaction data to construct the EXFOR database under the guidance of IAEA/NDS. Since the Asian nuclear reaction database workshop in 2017, there are a total of 11 entries produced for the EXFOR database, and these mainly include experimental data for isomeric yield ratio with the bremsstrahlung beam, the production cross sections by proton beams, and neutron total and capture cross sections. 6 of the total 11 entries were entered in the EXFOR DB, and 5 entries were reserved to enter into the EXFOR as Compiled status. The cross-sections of radionuclides produced from the ^{nat}Zr(p,x) reactions were determined using the stacked-foil activation method with the proton beam at the Korea Multi-purpose Accelerator Complex (KOMAC). The gamma-ray count of the produced radionuclides was measured using a HPGe detector and the monitor reaction of ^{nat}Cu(p,x)^{62}Zn was used to determine the proton beam flux. The present work was compared with literature data and the TENDL-2017 library.

1. EXFOR activity

EXFOR stands for the exchange format for experimental numerical nuclear reaction data. Nuclear reaction data produced by neutron, charged particle, and photon etc. goes through the EXFOR compilation process. The EXFOR compilation is basically performed with published nuclear data, using the EXFOR format rule. It will be completed in cooperation and agreement with IAEA/NDS and the NRDC network. The nuclear data will finally be disseminated to users through the EXFOR retrieval website. In other words, the EXFOR compilation is constructing the database of experimental nuclear data [1].

KAERI/NDC started the EXFOR compilation under the coordination of IAEA/NDS in 2009. Our responsibility is to compile the domestic nuclear data produced by neutron, charged particle and photon in Korea. Since 2009, we have produced a total of 80 entries, and 5 entries were compiled as shown in **Fig. 1**. Our center has made 8 entries on average per year. These entries mainly contain experimental data for neutron total cross section, the production cross sections induced by charged particles, and the photonuclear reaction using the bremsstrahlung beam.

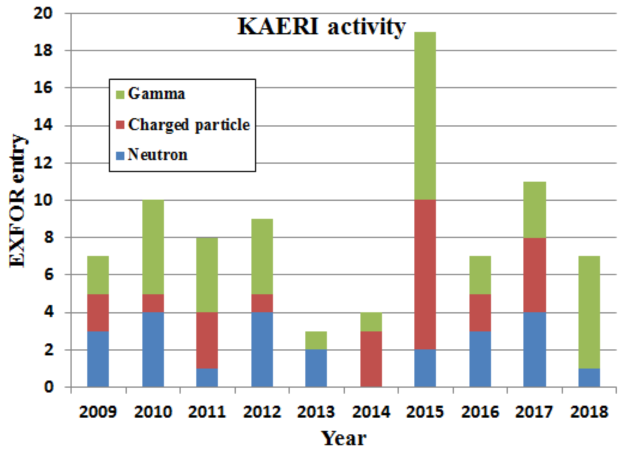

Fig. 1. EXFOR entries produced by KAERI/NDC for each year

Since the last Asian nuclear reaction database development workshop, a total of 11 entries were produced by our center. Six of these entries have entered the EXFOR database and 5 entries were compiled. We contacted the authors to obtain the numerical experimental data of the published articles for the EXFOR compilation. Cooperation with domestic experimental groups is very important for us to complete the compilation. We are working to maintain close relations with experimental groups through presentations and discussions at conferences or workshops related to nuclear data measurement.

2. Nuclear data measurement

Nuclear data is needed in various fields, for nuclear and fusion reactors, medical applications, radioisotope production, and accelerators etc. However, existing nuclear data have high uncertainty, and are not sufficient for use. It can have a negative effect on stability and calculations. To obtain accurate and precise nuclear data and improve safety and economy in nuclear technology and industrial applications, measurements are constantly needed.

We measured the production cross sections of the proton induced reaction on ^{nat}Zr using the stacked-foil activation method with the proton beam at the KOMAC facility. The production cross section of the proton induced reaction is useful for understanding the nuclear reaction mechanism, and for verification of nuclear theory. In addition, Zr is the target material used for the production of medical radioisotopes.

The activation experiment was carried out with the 57 and 69 MeV proton beam at KOMAC. Two stack assemblies were irradiated with the proton beams. One stack consisted of Cu, Y and Zr samples for the 57 MeV beam. The others stack was prepared in the order of Cu, Zr, and Al samples for 69 MeV proton irradiation. A high purity sample was used as the target and monitor and energy degrader. The HPGe detector was used to obtain the γ–ray count of the radionuclides produced from the ^{nat}Zr(p,x) reactions. The detection efficiency and energy calibration were obtained using the standard γ–ray sources. The cross sections of the proton induced reactions on ^{nat}Zr were determined by the well-known activation equation. The uncertainties of the measured cross sections were estimated by the square root of the quadratic sum of both statistical and systematic errors.

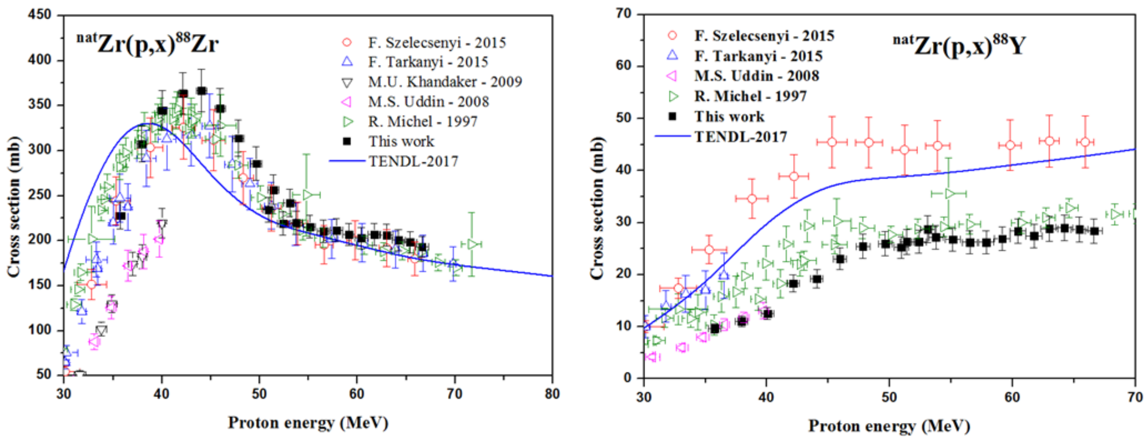

Fig. 2. Production cross sections of ^{88}Zr and ^{88}Y via the ^{nat}Zr(p,x) reactions.

The production cross sections of 13 radionuclides produced from the ^{nat}Zr(p,x) reactions were determined in this experiment. The measured data were compared with the literature data and the data from the TENDL-2017 library as shown in **Fig. 2**. The present results are in general agreement with existing experimental data, but some data showed inconsistent results. The details of this work are described in our paper [2].

References

[1] N. Otsuka et al., Nuclear Data Sheets **120** (2014) 272.

[2] S.C.Yang et al., Nucl. Instr. Meth. B **436** (2018) 179.

Evaluation of Photonuclear Cross Sections at KAERI

Young-Sik Cho

Nuclear Korea Atomic Energy Research Institute, 34057 Daejeon, Korea

Photonuclear data are very important and can be used for various fields of research and applications, including the production of medical radioisotopes, radiation shielding calculations and activation analyses. The current IAEA photonuclear data library [1] was generated in 1999 and includes the photonuclear reaction data for 164 isotopes. It has served as the primary resource for a variety of fields, but the need for its revision was raised by users because some data contains discrepancies with the recently measured data, and the evaluation techniques have been improved since then.

An IAEA CRP on updating the photonuclear data library and generating a reference database for photon strength functions is currently being conducted in collaboration with researchers in many countries. Under this CRP, the cross sections for 40 nuclides including ^{75}As, ^{93}Nb and ^{208}Pb were evaluated based on experimental/corrected data. The experimental data and corrected data were mainly collected from the EXFOR database. The OMP, level density parameters, GDR parameters and pre-equilibrium parameters were adjusted up to 20% of their default values, with some up to 50%, to fit to the experimental/corrected data. The model parameter tuning processes were automatically performed with the specially developed tuning tool (**Fig. 1**).

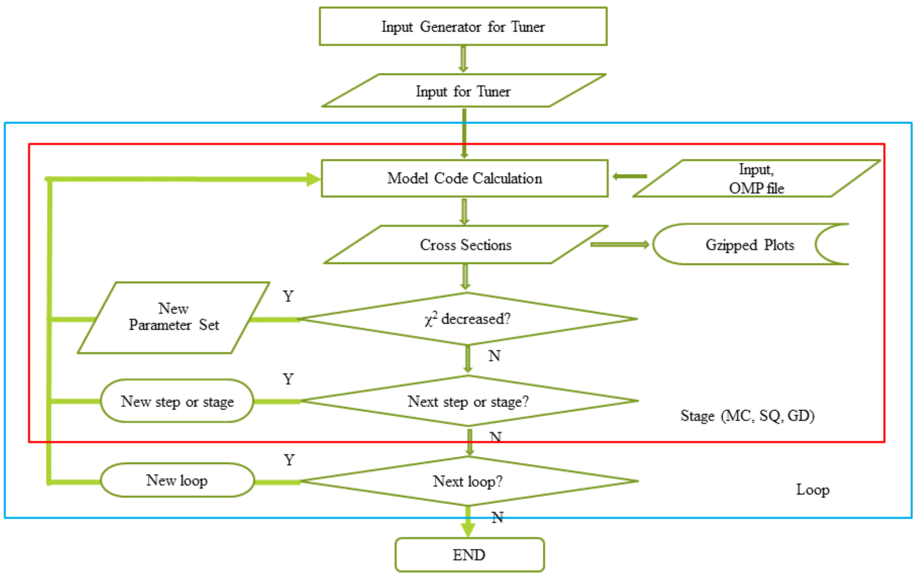

Fig. 1. Tuning procedure.

The calculated photonuclear cross sections for ^{159}Tb are shown in **Fig. 2**. Here the model parameters were adjusted to fit the calculations to the Fi-corrected data by Varlamov et al. [2-4].

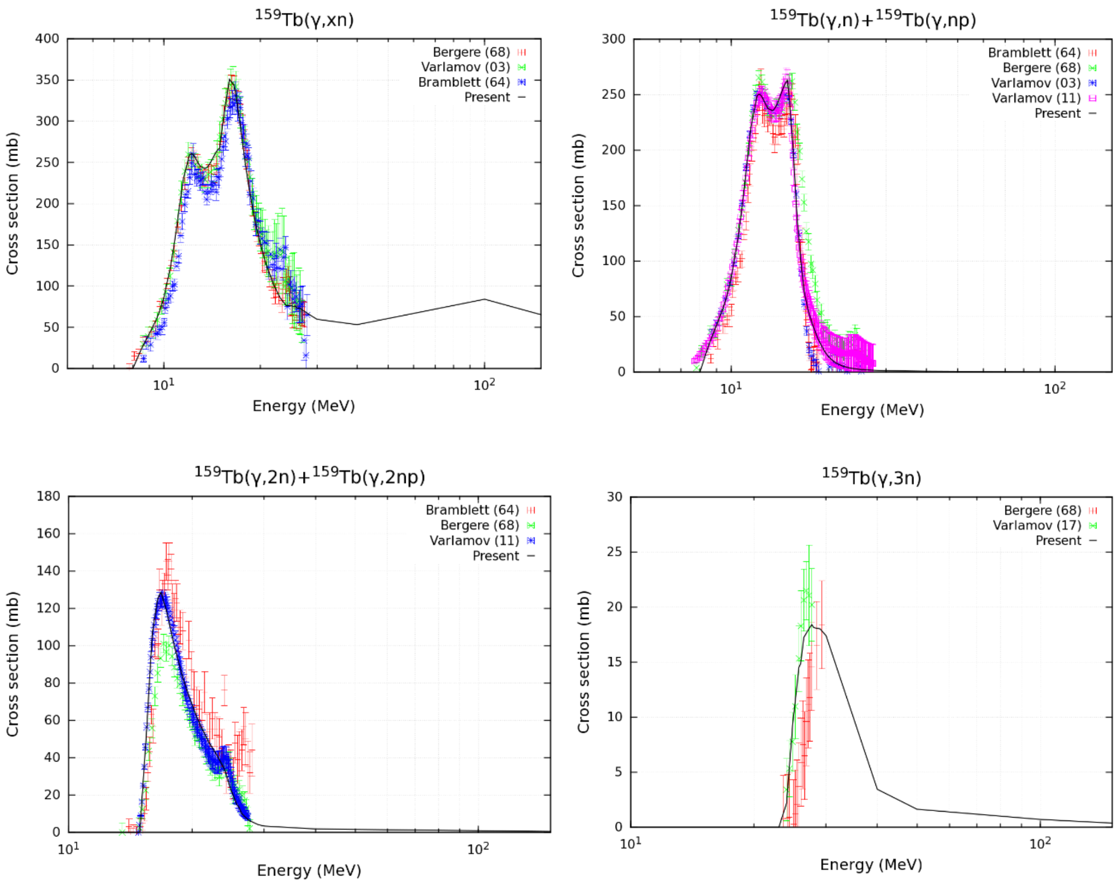

Fig. 2. The photonuclear cross sections for ^{159}Tb.

This work was partly supported by the IAEA CRP (Contract No. 20446).

References

[1] Handbook on photonuclear data for applications: Cross sections and spectra, IAEA-TECDOC-1178, 2000.

[2] V.V. Varlamov, N.N. Peskov, D.S. Rudenko, M.E. Stepanov, EXFOR M0635.

[3] V.V. Varlamov, B.S. Ishkhanov, V.N. Orlin, T.S. Polevich, M.E. Stepanov, EXFOR M0831.

[4] V.V. Varlamov, B.S. Ishkhanov, V.N. Orlin, EXFOR M0937.

Mass Yield Distribution in the ^{232}Th(n, *f*) Reaction Based on the ^{9}Be(p, n) Reaction Neutron

H. Naik[1], G.N. Kim[2], K. Kim[2], M. Zaman[2]

[1]*Radiochemistry Division, Bhabha Atomic Research Centre, Mumbai - 400 085, India*

[2]*Department of Physics, Kyungpook National University, Daegu 702-701, Korea*

The yields of fission products in the neutron, photon and charge particle induced fission of pre-actinides and actinides are needed for the mass and charge yield distributions to explain the basic physics such as the effect of nuclear-structure and the dynamics of descent from saddle to scission [1, 2]. In particular, the yields of fission products in the neutron induced fission of actinides are needed for decay heat [3] calculation and thus are important for the design of various types of reactors. The fission products yields in the neutron induced fission of ^{235}U, ^{238}U and ^{239}Pu are important for the conventional reactors (LWR, BWR) and fast reactor [4], On the other hand the yields of fission products in the neutron induced fission of ^{232}Th, ^{233}U and long-lived minor actinides (^{237}Np, ^{240}Pu, ^{241}Am, ^{243}Am, ^{244}Cm) are important for advanced heavy water reactor (AHWR) [5] and accelerated driven sub-critical system (ADSs) [6], respectively. In view of these facts, the cumulative yields of various fission products in the ^{232}Th(n, *f*) reaction with the average neutron energies of 7.46, 13.4 and 18.0 MeV have been measured by using an off-line γ-ray spectrometric technique. From the cumulative yields of the fission products, their mass-yields were obtained by using charge distribution correction [7, 8]. The mass yield distributions parameters such as peak-to-valley (P/V) ratio, average light mass ($\langle A_L \rangle$), heavy mass ($\langle A_H \rangle$) and the average neutron number ($\langle \upsilon \rangle$) were also obtained. The present and literature data [9-11] at in the ^{232}Th(n, *f*) reaction are compared with the similar data for the ^{238}U(n, *f*) reaction [12-14] available in EXFOR [15] to examine the role of excitation energy on the nuclear structure effect and on the mass distributions parameters.

The experiment was carried out by using the MC-50 Cyclotron at the Korean Institute of Radiological and Medical Sciences (KIRAMS), Korea. The fast neutrons were produced from the ^{9}Be(p, n) reaction by impinging the proton beam energies of 25, 35 and 35 MeV from the cyclotron on a 5-mm thick beryllium target. The neutron spectra from the ^{9}Be(p, n) reaction were generated by using a computer code MCNPX 2.6.0 [16]. From the neutron spectra, the average neutron energy ($\langle E_n \rangle$) within the range of threshold values to the maximum neutron energy ($\langle E_n \rangle$) were calculated by using the following equation.

$$\langle E_n \rangle = \int_{E_{th}}^{E_{\max}} E_n\, \phi(E_n)\, dE_n \Big/ \int_{E_{th}}^{E_{\max}} \phi(E_n)\, dE_n \,, \tag{1}$$

where $\phi(E_n)$ is the neutron flux as a function of neutron energy as obtained from MCNPx code [16]. The flux-weighted average neutron energies ($<E_n>$) based on the ^{9}Be(p, n) reaction for the three proton energies of 25, 35 and 45 MeV are 7.46, 13.4 and 18.0 MeV, respectively.

Three ^{232}Th metal foils with >99.99% purity, 0.025-mm thickness, and 192.3, 270.0 and 285.6 mg weight were separately wrapped with 0.025-mm thick pure Al foils. The target sample assemblies were fixed one at a time on a stand and placed on a proper height in air at a distance of 2.8 cm behind the Be-target. They were irradiated for 0.5 h, 1 h and 1 h each with the neutron beams generated from the bombardment of 45, 35 and 25 MeV proton beams on the Be target. The diameter of proton beam collimator was 10 mm. The proton beam current during irradiation for all the three experiments were about 200 nA. The irradiated ^{232}Th samples along with Al wrapper were taken out from the irradiated assembly after cooling time of 1.186 h, 0.605 h and 0.726 h, respectively. They were mounted on different Perspex (acrylic glass, 1.5 mm thick) plates. The γ-ray counting of the fission products from the Al wrapped ^{232}Th irradiated samples was done by using an energy- and efficiency-calibrated HPGe detector coupled to a PC-based 4K-channel analyzer. The resolution of the HPGe detector was 1.8 keV full-width at half-maximum (FWHM) at the 1332.5 keV γ-ray photo-peak of ^{60}Co. A standard source ^{152}Eu was used for the energy and the efficiency calibration.

From the total photo-peak activities, numbers of detected (N_{obs}) γ-rays for the fission products of interest were obtained by subtracting the linear Compton background. From N_{obs} of an individual fission product, the cumulative yields (Y_R) relative to ^{92}Sr were calculated by using the usual decay equation [10, 11],

$$Y_R = [\, N_{obs}\, (CL/LT)\, \lambda]\ n\, \sigma_f\ \ \varphi\, I_\gamma\, \varepsilon\, (1-e^{-\lambda t})\, e^{-\lambda T}\, (1-e^{-\lambda CL}) \tag{2}$$

where n is the number of target atoms, φ is the neutron flux and σ_f is the fluxed average fission cross section of ^{232}Th(n, f) reaction at the average neutron energies of 7.46, 13.4 and 18.0 MeV. I_γ is the γ-ray intensity [17], ε is the detection efficiency of the γ rays in the detector system and λ is the decay constant of the fission-product ($\lambda = \ln 2/T_{1/2}$). t and T are the irradiation and cooling times, whereas, CL and LT are the real time and the live time of counting, respectively.

From the Y_R values of the fission products, their relative mass-yields (Y_{RA}) were calculated by using the Wahl's prescription [7] after doing the charge distribution corrections [8]. The relative mass-yields (Y_{RA}) of the fission products obtained were then normalized to a total yield of 200% to calculate the absolute mass-yields (Y_A). The overall uncertainties in the yield were 4.3-14.5% is based on the contributions from counting statistics and systematic errors.

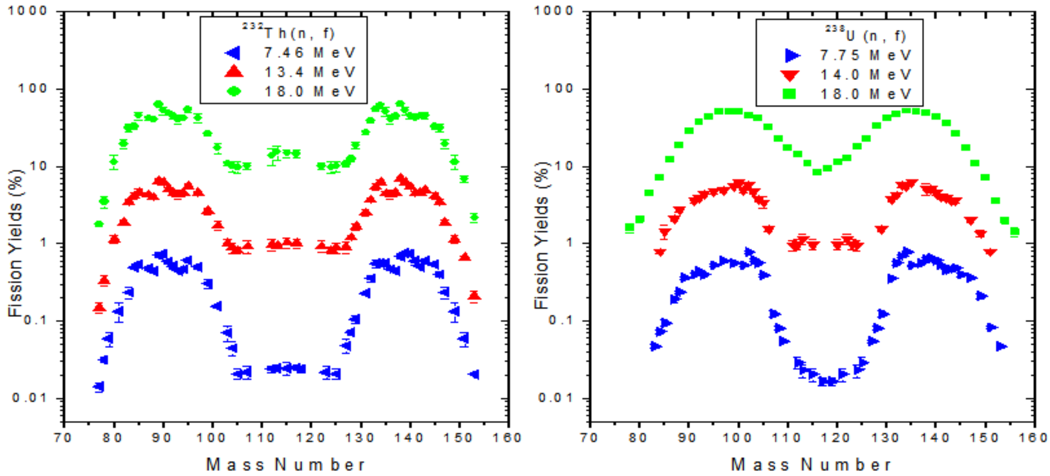

Fig. 1. Plot of mass yields in the ^{232}Th(n, *f*) reaction for the average neutron energies of 7.46, 13.4 and 18.0 MeV as well as in the ^{238}U(n, *f*) reaction for 7.75, 14.0 and 18.0 MeV.

The cumulative yields of asymmetric fission products in the ^{232}Th(n, *f*) reaction at the average neutron energies of 13.4 and 18.0 MeV are determined for the first time, whereas those of 7.46 MeV are the redetermined values but are in agreement with the literature data [9]. The mass-yield data in the ^{232}Th(n, *f*) reaction are plotted as a function of their mass number in **Fig. 1**. For comparison, the fission products yields in the ^{238}U(n, *f*) reaction at the neutron energies of 7.7, 14.0 and 18.0 MeV from literature [12-14] of comparable excitation energies are also plotted in the same figure. It can be seen from **Fig. 1** that within the neutron energy of 7.46-18 MeV, the mass yield distribution in the ^{232}Th(n, *f*) reaction is triple humped unlike in the ^{238}U(n, *f*) reaction, where it is double humped. This is due to the different type of potential energy surface between the two fissioning systems [18]. **Fig. 1** also shows that in both the ^{232}Th(n, *f*) and ^{238}U(n, *f*) reactions, the yields of fission products for A=133-134, 138-140,143-144 and their complementary products are higher than the other fission products. The oscillation of fission yields in the interval of five mass units around mass region of

133-144 and their complementary is due to the even-odd effect [19]. Besides this, the higher yields of fission products for A=134-134 and 143-144 are also due to the presence of spherical 82*n* and deformed 86–88*n* shells [20] based on the standard I and standard II asymmetric modes of fission [21].

From the mass-yields (Y_A) data, the average heavy mass ($<A_H>$) and the average light mass ($<A_L>$) in the ^{232}Th(n, *f*) reaction were calculated within the mass ranges of 80–105 and 125–150 or 124-149 (depending upon neutron energy) by using following relation.

$$<A_L> = \sum(Y_A A_L)/\sum Y_A, \qquad <A_H> = \sum(Y_A A_H)/\sum Y_A \tag{3}$$

From the $<A_L>$, $<A_H>$ and compound nucleus mass (A_C=233), the exact experimental average numbers of neutrons ($<\nu>_{expt}$) were calculated by using the following relation:

$$<\nu>_{expt} = A_C - (<A_L> + <A_H>) \tag{4}$$

The $<A_L>$and $<A_H>$values for the ^{232}Th(*n*, *f*) reaction from the present work and literature [9-11] as well as for the ^{238}U(*n*,*f*) reaction from Refs. [12-14] are plotted in Fig. 2, whereas the $<\nu>_{expt}$ values are plotted in Fig. 3 as a function of excitation energy. The average excitation energies ($<E^*>$) of the compound nucleus ^{233}Th* in the ^{232}Th(n, *f*) reaction were calculated from the average neutron energy ($<E_n>$), by using the following relation.

$$<E^*> = (\Delta_{232Th} + \Delta_n - \Delta_{233Th}) + <E_n> \tag{5}$$

where Δ is the mass excess taken from the Nuclear Wallet Cards [22]. For the compound nucleus ^{233}Th*, the average excitation energies corresponding to the average neutron energies of 7.46, 13.4 and 18.0 MeV are 12.07, 18.01 and 24.61 MeV, respectively.

Fig. 2 shows that at all excitation energy, the $<A_L>$ values in the ^{232}Th(*n*, *f*) reaction is significantly lower than in the ^{238}U(*n*, *f*) reaction, which is due to the mass conservation. However, the $<A_H>$ values are higher in the ^{232}Th(*n*, *f*) reaction than in the ^{238}U(*n*, *f*) reaction. This is most probably due to favorable standard II asymmetric mode compared to standard I asymmetric mode of fission in the ^{232}Th(*n*, *f*) reaction than in the ^{238}U(*n*, *f*) reaction. **Fig. 2** also shows slight increasing trend of $<A_L>$ and decreasing trend of $<A_H>$, which is due to the variation of yields for A=133-134, 139-140 and 143-144 with excitation energy.

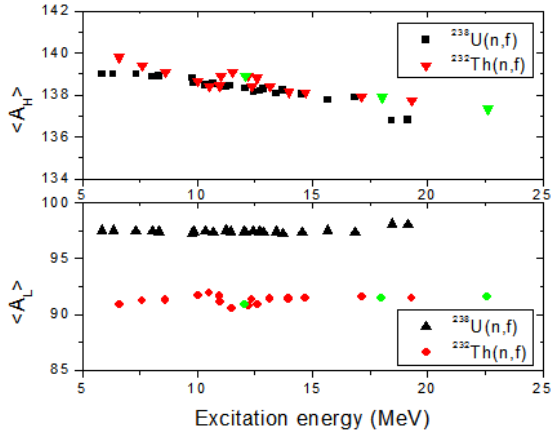

Fig. 2. $\langle A_H \rangle$ and $\langle A_L \rangle$ as a function of $\langle E^* \rangle$ in the ^{232}Th(n,*f*) and ^{238}U(n,*f*) reactions. Present data in green color.

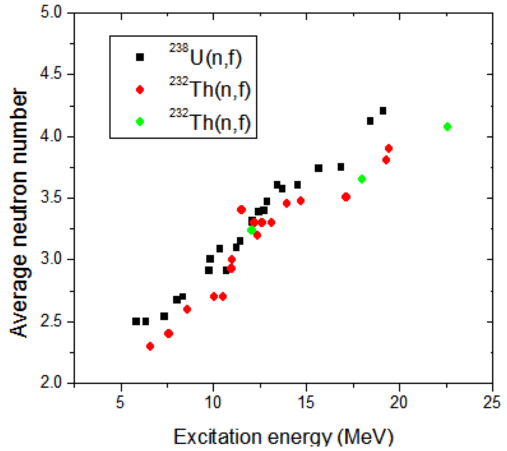

Fig. 3. Plot of $\langle \upsilon \rangle$ value as a function of <E8> in the ^{232}Th(n,*f*) and ^{238}U(n,*f*) reactions. Present data in green color.

The role of excitation energy can be very well seen from **Fig. 3**. The $\langle \nu \rangle_{expt}$ value in both the ^{232}Th(*n*, *f*) and ^{238}U(*n*, *f*) reactions increases with excitation energy. **Fig. 3** also shows that the $\langle \nu \rangle_{expt}$ value in the ^{232}Th(*n*, *f*) reaction is lower than in the ^{238}U(*n*, *f*) reaction, which is due to the difference in fissility parameter. The role of excitation can be also seen from the plot of highest asymmetric product and symmetric products (**Fig. 4**) and their ratio i.e. the peak-to valley (P/V) ratio (**Fig. 5**). It can be seen from **Fig. 4** that in both the ^{232}Th(n, *f*) and ^{238}U(n, *f*) reactions, the yields of asymmetric products decrease slightly, whereas the yields of symmetric products increase significantly with excitation energy. Accordingly, the peak-to valley (P/V) ratio decreases sharply with excitation energy. It can also be seen from Fig. 4 that the yields of symmetric products below the excitation energy of 7.5 MeV are lower in the ^{232}Th(n, *f*) reaction than in the ^{238}U(n, *f*) reaction. Above the excitation energy of 7.5 MeV, the yields of symmetric products are higher in the ^{232}Th(n, *f*) reaction than in the ^{238}U(n, *f*) reaction. This observation indicates that the increase trend of yields for symmetric fission products and decrease trend of P/V ratio with excitation energy is more sharper in the ^{232}Th(n, *f*) reaction than in the ^{238}U(n, *f*) reaction [23]. This is due to the different type of potential energy surface [18] in ^{233}Th* compared to ^{239}U* as mentioned before besides the role of excitation energy.

The authors would like to express their sincere thanks to the staff of the MC-50 Cyclotron in the KIRAMS for the excellent operation and their support during the experiment. This research was partly supported by the Institutional Activity Program of

KAERI, 2017, by the National Research Foundation of Korea through a grant provided by the Ministry of Science, ICT & Future Planning (NRF-2017R1D1A1B03030484), and by the National R&D Program through the Dong-nam Institute of Radiological and Medical Sciences (50496-2017). One of the authors (H. Naik) was supported by the Korean Brain Pool Program (No. 171S-1-3-1786) of Korean Federation of Science and Technology Societies (KOFST).

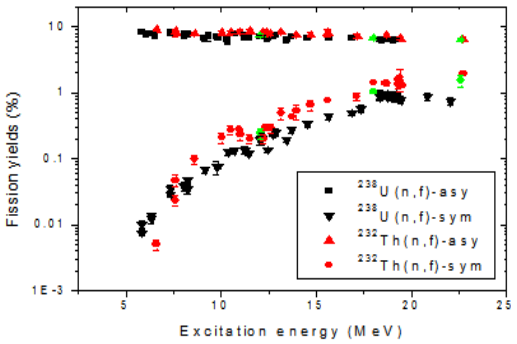

Fig. 4. Yields of symmetric and asymmetric products vs. <E*> in the ^{232}Th(n,*f*) and ^{238}U(n,f) reactions. Present data in green color.

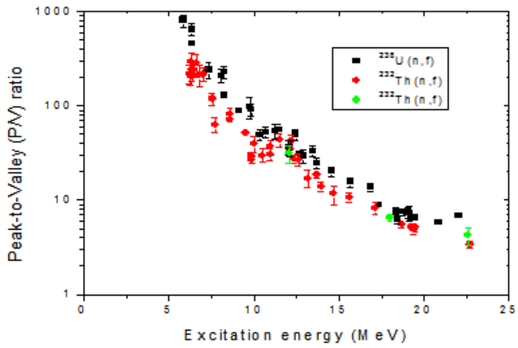

Fig. 5. P/V ratio vs. <E8> in the ^{232}Th(n, *f*) and ^{238}U(n, *f*) reactions. The present data are of green color.

References

[1] R.Vandenbosch and J.R.Huizenga, Nuclear Fission (Academic, New York, 1973).

[2] U. Brossa, S. Grossmann, A. Muller, Phys. Rep. **197** (1990) 167.

[3] K. Oyamatsu, H. Takeuchi, M. Sagisaka, J. Katakura, J. Nucl. Sci. Tech. **38** (2001) 477.

[4] T.R. Allen, D.C. Crawford, Lead-cooled fast reactor systems and the fuels and materials challenges, Sci. Technol. Nucl. Install. (2007), Article ID 97486.

[5] R.K. Sinha, A. Kakodkar, Nucl. Eng. Des. **236** (2006) 683.

[6] F. Carminati, R. Klapisch, J.P. Revol, Ch. Roche, J.A. Rubia, C. Rubia, An energy amplifier for cleaner and inex-haustible nuclear energy production Driven by particle beam accelerator, CERN/AT/93-49 (ET) 1993.

[7] A.C. Wahl, At. Data Nucl. Data Tables **39** (1988) 1.

[8] H. Umezawa, S. Baba, H. Baba, Nucl. Phys. A **160** (1971) 65.

[9] L.E. Glendenin, J.E. Gindler, I. Ahmad, D.J. Henderson, J.W. Meadows, Phys. Rev. C **22** (1980) 152.

[10] H. Naik, Rita Crasta, S.V. Suryanarayana, P.M. Prajapati, V.K. Mulik, B.S. Shivasankar, K.C.Jagadeesan, S.V.Thakare, S.C.Sharma and A.Goswami, Eur. Phys. J. A. **50** (2014) 144.

[11] H. Naik, Sadhana Mukherji, S.V. Suryanarayana, K.C. Jagadeesan, S.V. Thakare and S.C. Sharma, Nucl. Phys. A **952** (2016) 100.

[12] S.Nagy, K.F.Flynn, J.E.Gindler, J.W.Meadows, L.E.Glendenin, Phys. Rev. C **17** (1978) 163.

[13] H. Naik, V.K. Mulik, P.M. Prajapati, B.S. Shivasankar, S.V. Suryanarayana, K.C. Jagadeesan, S.V. Thakare, S.C. Sharma, A. Goswami, Nucl. Phys. A **913** (2013) 185.

[14] H. Naik, Sadhana Mukerji, Rita Crasta, S.V. Suryanarayana, S.C. Sharma and A. Goswami, Nucl. Phys. A **941** (2015) 16.

[15] IAEA-EXFOR Database, available at http://www-nds.iaea.org/exfor.

[16] J.S. Hendricks, W.M. Gregg, L.F. Michael, R.J. Michael, C.J. Russell, W.D. Joe, P.F. Joshua, B.P. Denise, S.W. Laurie, W.M. William, MCNPX 2.6.0 Extensions, LANL Report LA-UR-08-2216, Los Alamos, 2008, available from: http://mcnpx.lanl.gov/.

[17] NuDat 2.6, National Nuclear Data Center, Brookhaven National Laboratory, updated 2011, Available from: http://www.nndc.bnl.gov/.

[18] P. Moller, Nucl. Phys. A **192** (1972) 529.

[19] H. Naik, R.J. singh and R.H. Iyer, The European Physical Journal A **16** (2003) 495.

[20] B.D. Wilkins, E.P. Steinberg, R.R. Chasman, Phys. Rev. C **14** (1976) 1832.

[21] U. Brossa, S. Grossmann, A. Muller, Phys. Rep. **197** (1990) 167.

[22] J. K. Tuli, Nuclear Wallet Cards (2011) [www.nndc.bnl.gov].

[23] I.V. Ryzhov, S.G. Yavshits, G.A. Tutin, N.V. Kovalev, A.V. Saulski, N.A. Kudryashev, A.V. Saulski, N.A. Kudryashev, M.S. Onegin, L.A. Vaishnene, Yu.A. Gavrikov, O.T. Grudzevich, V.D. Simutkin, S. Pomp, J. Blomgren, M. Osterlund, P. Andersson, R. Bevilacqua, J. Meulders, R. Prieels, Phys. Rev. C **83** (2011) 054603.

Study of Nuclear Reactions $^{141}Pr(\gamma,2n)^{139}Pr$ and $^{141}Pr(\gamma,pn)^{139}Ce$ with Bremsstrahlung End-point Energy in the Range 50-70 MeV

Nguyen Van Do[1,3], Nguyen Thi Xuan[2], Nguyen Thanh Luan[3], Nguyen Thi Hien[4], Guinyun Kim[4]

[1]*Institute of Theoretical and Applied Research, Duy Tan University, 73 Hoang Cau Street, Hanoi, Vietnam,*

[2]*Graduate School of Science and Technology, VAST, 18 Hoang Quoc Viet, Hanoi, Vietnam.*

[3]*Institute of Physics, Vietnam Academy of Science and Technology, 10 Dao Tan, Ba Dinh, Hanoi, Viet Nam.*

[4]*Department of Physics, Kyungpook National University, Daegu 41566, Republic of Korea.*

Abstract

The photonuclear reactions $^{141}Pr(\gamma,2n)^{139}Pr$ and $^{141}Pr(\gamma,pn)^{139}Ce$ induced in the same praseodymium foils bombarded with 50-, 60-, and 70-MeV bremsstrahlung end-point energies were investigated. The integrated cross sections for the formation of the two isobars ^{139}Pr and ^{139}Ce were determined relative to that of the reference reaction $^{141}Pr(\gamma,2n)^{139}Pr$. The measurements were carried out by the activation method in combination with the off-line γ-ray spectrometry. The experimental results are compared with the theoretical predictions using the code TALYS 1.8. The experiment was performed at the Pohang electron linac of the Pohang Accelerator Laboratory (PAL), POSTECH, Pohang, Korea.

Keywords: Integrated cross section, $^{141}Pr(\gamma,2n)^{139}Pr$ and $^{141}Pr(\gamma,pn)^{139}Ce$ reactions, Activation, γ-ray spectrometry.

1. Introduction

In recent years, the studies of photonuclear reaction have been increasingly conducted thanks to the fast development of the bremsstrahlung radiation sources based on the electron linac. Analysis of the photonuclear reaction data can help to broaden our understanding of the basic aspects of nuclear reaction mechanisms, confirmation of the validity of the nuclear models and contribution to the different fields of application. Most of the photonuclear reaction studies were performed in the Giant Dipole Resonance (GDR) energy range (≤ 30 MeV) [1-4], where only simple photonuclear reactions occur and the reaction mechanism can be fairly well explained in terms of the compound nuclear model. However, beyond the GDR energy region, multiparticle photoreaction channels can also open and the understanding of these nuclear reaction mechanisms are still not sufficient. Therefore, the study of nuclear reaction at energies beyond the GDR region is gaining much attention [5-9].

In this work we have investigated the $^{141}Pr(\gamma,2n)^{139}Pr$ and $^{141}Pr(\gamma,pn)^{139}Ce$ reactions, and determined their integrated cross sections. We have chosen these reactions for the studies because there was no earlier investigation. In addition, the ^{139}Ce has a potential as a calibration source for SPET, and the ^{139}Pr produced from the $^{141}Pr(\gamma,2n)^{139}Pr$ reaction is a positron generator and thus has the potential as a PET radiotracer. Usually, the ^{139}Pr isotope is obtained from the $^{140}Ce(p,2n)^{139}Pr$ and $^{141}Pr(p,3n)^{139m}Nd \rightarrow ^{139}Pr$ reaction processes, so its production in the $^{141}Pr(\gamma,2n)^{139}Pr$ reaction is considered as one of the complementary methods.

2. Experimental

The bremsstrahlung radiations used in this study were produced by the bombardment of the accelerated electron beam into a thin (0.1 mm) tungsten (W) target with a size of 100 mm × 100 mm, which was placed at a distance of 15 cm from the electron beam exit window. Three praseodymium metallic foils with purity of 99.9%, thickness of 0.10 mm, and size of 15 mm x 15 mm were irradiated separately with the bremsstrahlung end-point energies of 50-, 60-, and 70-MeV for about one hour. During each irradiation, the electron beam current was kept stable, with fluctuation around 6%. In order to follow the changes of the beam current, the integrator counts were also recorded in multichannel scaling mode for the correction of photon flux fluctuation, if it is necessary. The photonuclear reactions considered in this investigation are given in **Table 1** [10].

The gamma-ray spectra were recorded using a well calibrated HPGe detector (ORTEC-GEM-20180-p). The HPGe detector was coupled to a PC based 4 K channel analyzer card system. The relative efficiency of the detector is 20% and the energy resolution is 1.8 keV at the 1332.5 keV gamma-ray peak of ^{60}Co. The energy-dependent efficiency of the detector was determined by using a set of calibrated gamma-ray sources. For the γ-ray spectrum measurements the dead-time was kept under 5%. Because the half-lives of radioactive nuclides formed in the same praseodymium foil is a large difference, a number of γ-ray spectra were measured to follow the decay of the considered reaction products. The length of the measuring time was chosen depending on the statistics of the photopeak of interest. Typical gamma-ray spectra of the irradiated praseodymium foil taken at different waiting times are given in **Figs. 1** (a,b,c). In the activity measurements, the intense γ-rays were chosen and the necessary interference corrections were made. For the activity measurement of the ^{139}Ce, the contribution of the ^{139}Pr via EC decay was corrected.

Table 1. Main nuclear decay data of the investigated reaction products [10].

Reaction	E_{th} (MeV)	$T_{1/2}$	Decay mode (%)	Main γ-ray keV	Intensity %
^{141}Pr(γ,n)^{140}Pr	9.40	3.39(1) m	EC (100)	306.9(5) 1596.1(2)	0.147(19) 0.49
^{141}Pr(γ,2n)^{139}Pr	17.34	4.41(4) h	EC (100)	1347.33(2) 1630.67(2)	0.473 0.343(12)
^{141}Pr(γ,p2n)^{139m}Ce	14.43	54.8(10) s	IT (100)	754.24(8)	93(9)
^{141}Pr(γ,p2n)^{139g}Ce	14.43	137.640(20) d	EC (100)	165.8575(11)	80(8)
^{27}Al(γ,2pn)^{24}Na	23.71	14.997(12) h	β^- (100)	1368.626(5)	99.9936(15)

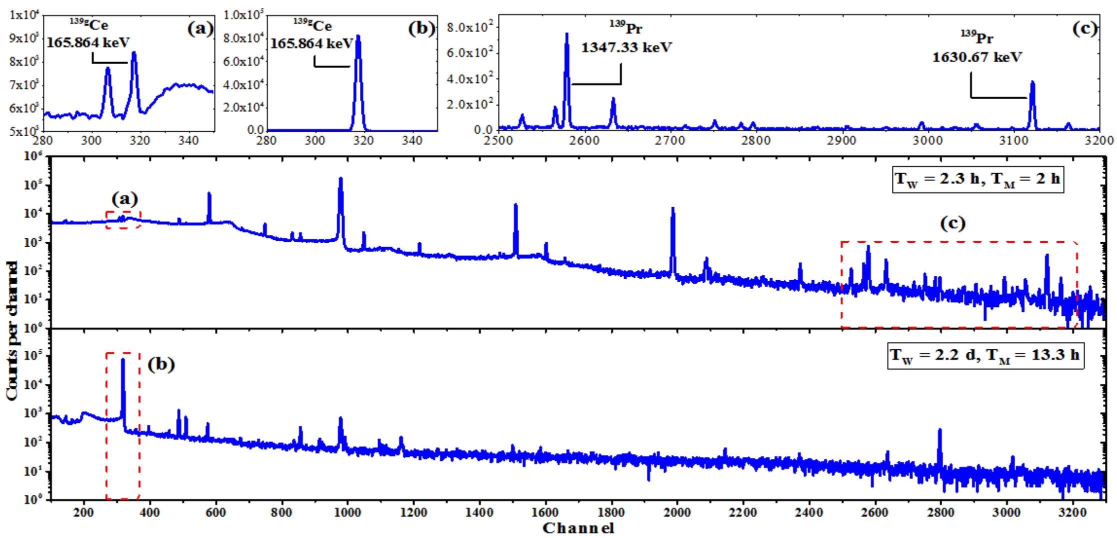

Fig. 1(a, b, c). Typical γ-ray spectra of the irradiated ^{141}Pr measured at different waiting times.

3. Data analysis

The yield of the photonuclear reaction is expressed as follows:

$$Y_i = \int_{E_{th}}^{E_{\gamma\max}} \sigma_i(E)\phi(E)dE \tag{1}$$

where i represents the nuclear reaction of interest, $\sigma_i(E)$ is the energy dependent reaction cross section and $\phi(E)$ is the shape of the bremsstrahlung spectrum. $E_{\gamma max}$ and E_{th} are the bremsstrahlung maximum end-point energy and the reaction threshold energy, respectively. The reaction yield can be determined via the measured activity of the reaction product:

$$Y = \left(\lambda N_\gamma f\right) / \left(N_0 F \varepsilon_\gamma I_\gamma\right) \tag{2}$$

$$F = \left[\left(1-e^{-\lambda\tau}\right)/\left(1-e^{-\lambda T}\right)\right] e^{-\lambda(T-\tau)} \left(1-e^{-\lambda t_i}\right) e^{-\lambda t_w} \left(1-e^{-\lambda t_c}\right) \tag{3}$$

where λ is the decay constant of the radioactive isotope, N_γ is the counting number under the photopeak, f is the correction factor for the counting losses, N_0 is the number of target nuclei, ε_γ is the absolute efficiency of the γ-ray detector, I_γ is the branching ratio of the gamma ray, τ is the pulse width, t_i, , t_w, and t_c are the irradiation time, waiting and counting time, respectively. T is the cycle period.

In practice, the integrated reaction cross section can be evaluated by direct integration of the cross-section curves from the threshold energy to the bremsstrahlung end-point energy or derived from the reaction yield. In this work, we determined the integrated cross sections (x) of the ^{141}Pr(γ,2n)^{139}Pr and ^{141}Pr(γ,pn)^{139}Ce based on the monitor (m) reaction ^{141}Pr(γ,n)^{140}Pr [11] as follows:

$$Y_{(x)} / Y_{(m)} = k \times \sigma_{\text{int},(x)} / \sigma_{\text{int},(m)} \tag{4}$$

In which, the k factor presents to the thresholds of the two different reactions, (x) and (m), respectively. The value of k was determined as follow:

$$k = \bar{\phi}_{W,(x)} / \bar{\phi}_{W,(m)} \tag{5}$$

where $\bar{\phi}_{W,i}$ is so called the weighted average flux, and its value can be obtained by calculations as follows:

$$\bar{\phi}_{W,i} = \int_{E_{th}}^{E_{\gamma max}} \sigma_i(E)\phi(E)dE \,/ \int_{E_{th}}^{E_{\gamma max}} \sigma_i(E)dE \qquad (6)$$

In this work, the energy dependent cross sections were calculated using the code TALYS 1.8 [12] and the bremsstrahlung spectrum was estimated using the MCNPX code [13].

In order to check the validity of the present experimental procedure we have determined the integrated cross section of the ^{141}Pr(γ,n)^{140}Pr relative to that of the ^{27}Al(γ,2pn)^{24}Na [14]. The obtained integrated cross sections of the ^{141}Pr(γ,n)^{140}Pr reaction for bremsstrahlung end-point energies 50-,60-, and 70-MeV differ from the measurements of Cook et al., [11] in the range 6-13%.

3. Results and discussion

By applying the proposed experimental procedure we have measured the integrated cross sections for the ^{141}Pr(γ,2n)^{139}Pr and ^{141}Pr(γ,pn)^{139}Ce reactions. The obtained results are given in **Table 2**. The total uncertainties for the ^{141}Pd(γ,2n)^{139}Pr and ^{141}Pd(γ,pn)^{139}Ce reactions are around 11-13% and 15-18%, respectively. From **Table 2** we can see that in the bremsstrahlung end-point energy range 50-70 MeV the integrated cross sections of the ^{141}Pd(γ,2n)^{139}Pr reaction are about more than one order of magnitude higher compared to that of the ^{141}Pd(γ,pn)^{139}Ce reaction. We are unable to compare the present results with reference data because there was no previous measurement. For comparison we have calculated the integrated cross sections using the code TALYS 1.8 [12]. The calculations were performed with six level density models [12]. Both the experimental and calculated results are illustrated in **Fig. 2**. As visually, the experimental results and theoretical predictions are in agreement within the error limits.

Table 2. The integrated cross sections of the ^{141}Pr(γ,2n)^{139}Pr and ^{141}Pr(γ,pn)^{139}Ce reactions.

Residual product	Integrated cross section (MeV-mb)					
	Experimental			TALYS calculation		
	50 MeV	60 MeV	70 MeV	50 MeV	60 MeV	70 MeV
^{139}Pr	382.34±49.71	416.52±50.98	451.35±52.98	385.74	400.18	411.46
^{139}Ce	12.12±2.14	20.40±3.18	25.56±3.76	13.67	19.53	24.66

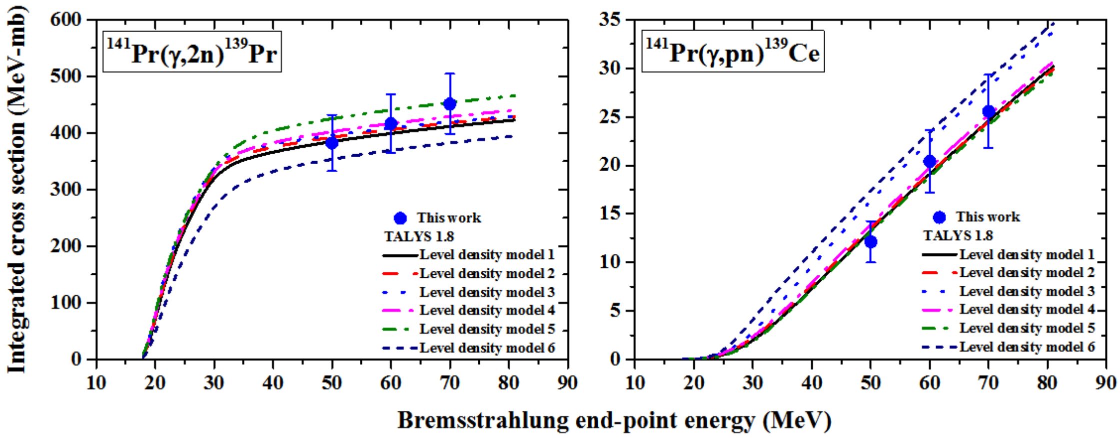

Fig. 2. The integrated cross sections of the ^{141}Pr(γ,2n)^{139}Pr and ^{141}Pr(γ,pn)^{139}Ce reactions.

References

[1] Y.P. Gangrsky et al., Phys. Atom. Nuclei. **67** (2004) 1227.

[2] I.N. Vishnevsky et al., Phys. Rev. C **79** (2009) 014615.

[3] V.M. Mazur et al., Int. J. Mod. Phys. E **20** (2011) 2329.

[4] T.D. Thiep et al., J. Radional. Nucl. Chem. **311** (2017) 887.

[5] T. Kato et al., J. Radioanal. Chem. **32** (I 976) 51.

[6] Jozsef Safar, Laszlo Lakosi, Radiat. Phys. Chem. **95** (2014) 26.

[7] S.S. Belyshev et al., Eur. Phys. J. A (2015) 51: 67

[8] Nguyen Van Do et al., Appl. Radiat. Isot., **128** (2017) 148.

[9] Nguyen Van Do et al., Radiat. Phys. Nucl. Chem., **149** (2018) 54.

[10] NuDat 2.6, National Nuclear Data Center, Brookhaven National Laboratory, updated 2011, Available on <http://www.nndc.bnl.gov/>.

[11] B. C. Cook et al., Phys. Rev., **143** (1966) 730.

[12] A.J. Koning, S. Hilaire, S. Goriely, 2015. TALYS 1.8, <http://www.talys.eu/download-talys/>.

[13] J.S. Hendricks, W.M. Gregg, L.F. Michael, R.J. Michael, C.J. Russell, W.D. Joe, P.F.P.F. Joshua, B.P. Denise, S.W. Laurie, W.M. William, 2008, MCNPX 2.6.0 Extensions, LANL Report LA-UR-08-2216, Los Alamos, <http://mcnpx.lanl.gov>.

[14] R.A. Mayer et al., Nucl. Phys. A**122** (1968) 606.

KAERI Neuron Time-of-flight (nTOF) Facility – Introduction and Current Status

Jong Woon Kim* and Young-Ouk Lee

Korea Atomic Energy Research Institute, 1045 Daedeokdaero, Yuseong-gu, Daejeon, Korea, 305-353

The project for building a neutron time-of-flight facility was initiated after the Nuclear Data Center was established in December 2011 at KAERI. This consists of two main parts. One is constructing the nTOF measurement building, and the other is generating a pulsed neutron beam by repairing the existing superconducting accelerator and making a photo-neutron source.

Unlike equipment manufacturing and repair, construction of the nTOF measurement building was considerably delayed due to budget and various licensing issues. However, finally, the construction of nTOF measurement building was started in May 2018 and will be completed by the end of this year.

This building simply makes up of a measurement hall and rooms for measured data processing and analysis.

Pulsed neutron beam are produced by bremsstrahlung photons through (γ,n) reactions by stopping the incident electrons in a liquid lead target. For this, electron beam is produced by the KAERI superconducting accelerator in the neighboring building. The expected electron beam operating conditions are 17 MeV, average current 0.08mA, and 20ps pulse width with 200 kHz.

In this presentation, the introduction of KAERI neutron time-of-flight facility and current status will be presented.

The First Unbound States of Mirror ^{9}B and ^{9}Be Nuclei in the Complex Scaling Method

M.Odsuren[1], Y.Kikuchi[2], T.Myo[3,4], K.Katō[5]

[1]*School of Engineering and Applied Sciences, National University of Mongolia, Ulaanbaatar 210646, Mongolia*

[2]*General Education, Tokuyama College, National Institute of Technology, Shunan 745-8585, Japan*

[3]*General Education, Faculty of Engineering, Osaka Institute of Technology, Osaka 535-8585, Japan*

[4]*Research Center for Nuclear Physics (RCNP), Osaka University, Ibaraki 567-0047, Japan*

[5]*Nuclear Reaction Data Centre, Faculty of Science, Hokkaido University, Sapporo 060-0810, Japan*

The structures of the first $1/2^+$ unbound states of A=9 mirror nuclei are studied in the complex scaled $\alpha+\alpha+N$ three-body model. The result indicates that the $1/2^+$ state of ^{9}Be is a virtual state of the s-wave neutron around the ^{8}Be (two-alpha) core. But the analog ^{9}B($1/2^+$) state is predicted as a resonant state due to the Coulomb barrier.

1. Introduction

A study of mirror nuclei plays an important role in understanding of the nuclear structure. The properties of mirror nuclei ^{9}Be and ^{9}B are investigated within a framework the α+α+n three-body model using of the complex scaling method (CSM) [1-2]. There have been considerable experimental and theoretical efforts to determine the energy levels of the low-lying states of ^{9}Be and ^{9}B, specially the first unbound $1/2^+$ states.

We investigated the photodisintegration cross section of the reaction of ^{9}Be(γ,n) and also discussed the structure of the excited $1/2^+$ state of ^{9}Be by applying the CSM to the α+α+n three-body model. From the decomposition of the photodisintegration cross section into the available three-body final states, it was found that the $1/2^+$ state decays into the ^{8}Be(0^+)+n continuum states dominantly, indicating the possibility of the virtual-state nature of the first excited $1/2^+$ state [3].

It is particularly interest to compare the structure of the ^{9}Be($1/2^+$) state with the same spin parity state of the mirror nucleus ^{9}B. In this study, we discuss the structure of the first excited $1/2^+$state of ^{9}B together with the mirror state in ^{9}Be. Considering the virtual and resonance characters of the *s*-wave states in *A*=9 systems, we investigate the nature of the first excited $1/2^+$ states of ^{9}Be and ^{9}B mirror nuclei.

2. Theoretical framework

2.1. Three-body model

The Hamiltonian for the relative motion of the α+α+N (N=p or n) three-body system for mirror ^{9}Be and ^{9}B nuclei are given as

$$\hat{H} = \sum_{i=1}^{3} t_i - T_{c.m.} + \sum_{i=1}^{2} V_{\alpha N}(\xi_i) + V_{\alpha\alpha} + V_{3b} + V_{PF}, \tag{1}$$

where t_i and $T_{c.m.}$ are kinetic energy operators for each particle and the center-of-mass of the system, respectively. The interactions between the nucleon and the i-th α particle is given as $V_{\alpha N}(\xi_i)$, where ξ_i is the relative coordinate between them. We employ the KKNN [4] potential for $V_{\alpha N}$. The potential $V_{\alpha\alpha}$ is the α-α interaction and we apply a folding potential [5] of the effective nuclear and Coulomb forces. The pseudopotential V_{PF} is the projection operator to remove the Pauli forbidden states from the relative motions of α-α and α-N. In addition to the two-body interactions $V_{\alpha N}$ and $V_{\alpha\alpha}$, which are fixed so as to reproduce the experimental properties of the α-N and α-α subsystems, we introduce the three-body potential V_{3b} such as

$$V_{3b}=V_3 \exp(-\mu\rho^2), \tag{2}$$

where ρ is the hyperradius of the α+α+N three-body system, V_3 and μ are the strength and width of the three-body potential, respectively.

2.2. Complex scaling method

The complex-scaled *Schrödinger* equation is expressed using the complex-scaled Hamiltonian $\hat{H}^\theta$ as

$$\hat{H}^\theta \psi_J^\nu(\theta) = E\psi_J^\nu(\theta), \tag{3}$$

where J is the total spin of the α+α+N and ν is the state index. The relative coordinates $\vec{r}_i$ of the three-body α+α+N system are transformed as $\vec{r}_i \rightarrow \vec{r}_i e^{i\theta}$ $(i=1,2)$ with a real parameter θ. The $U(\theta)$ operates on the function ψ_J^ν, that is,

$$\psi_J^\nu(\theta) = U(\theta)\psi_J^\nu(\vec{r}_1,\vec{r}_2) = e^{\frac{3}{2}i\theta \cdot 2}\psi_J^\nu(\vec{r}_1 e^{i\theta},\vec{r}_2 e^{i\theta}). \tag{4}$$

The complex scaled Hamiltonian of inter cluster motion is given by

$$\hat{H}^\theta = U(\theta)\hat{H}U^{-1}(\theta). \tag{5}$$

3. Results

In **Fig. 1**, we show the calculated cross sections in comparison with the two sets of the observed data [6, 7] which commonly have peaks just above the ^{8}Be+n threshold. To reproduce the measured data, we apply the three-body potential with $V_3 = -1.02$ MeV and $\mu = 0.02$ fm^{-2} in Eq. (2). We confirm that the calculated cross section rapidly increases just above the ^{8}Be+n threshold and there is negligibly small strength below this threshold. We have also found that the calculated cross sections show the strong dependence on the strengths of the three-body potentials [4]. The origin of the low-lying peak of the cross section above the ^{8}Be+n threshold is investigated to be a consequence of a ^{8}Be+n virtual state but not resonant one.

In **Fig. 2**, we show the distribution of the energy eigenvalues for the $1/2^+$ state calculated with the same parameters used in the photo-disintegration calculations. We could not find a sharp resonance corresponding to the $1/2^+$ peak in the cross section using the CSM calculation.

In **Fig. 3**, we show the distribution of the energy eigenvalues for the $1/2^+$ state in ^{9}B calculated with $V_3 = -1.02$ MeV, which reproduces the photo-disintegration of ^{9}Be, in the α+α+p model. We find a resonance solution at the energy $E_{res} = 2.42$ MeV with a decay width $\Gamma = 1.61$ MeV, which is presented with a triangle in **Fig. 3**. In a recent compilation data [6] Tilley *et al.* have reported that the $1/2^+$ state of ^{9}B is a resonance state with $E_{res} = 1.6$ MeV and $\Gamma = 0.77$ MeV. In comparing the calculated result with experiment, our calculated energy with a decay width gives higher values than measured data. To study out this, it would be important to perform further analysis for structure of the $1/2^+$ state of ^{9}B.

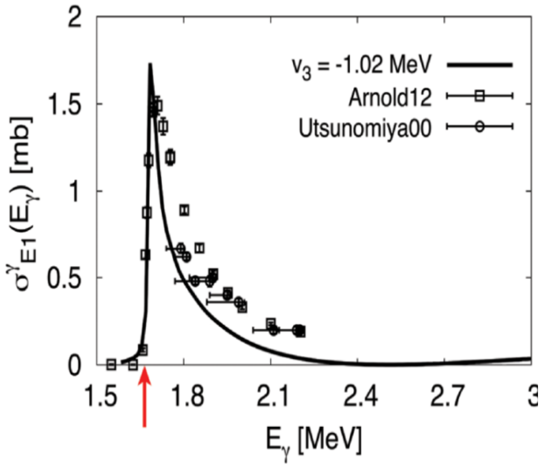

Fig. 1. Calculated photodisintegration cross sections in comparison with the experimental data. The experimental data are taken from Refs. [7] and [8]. The arrow indicates the threshold energy of the ^{8}Be(0^{+})+n channel. The black (solid) line represents the cross section calculated by using an attractive three-body potential with $\boldsymbol{V_3 = -1.02}$ MeV.

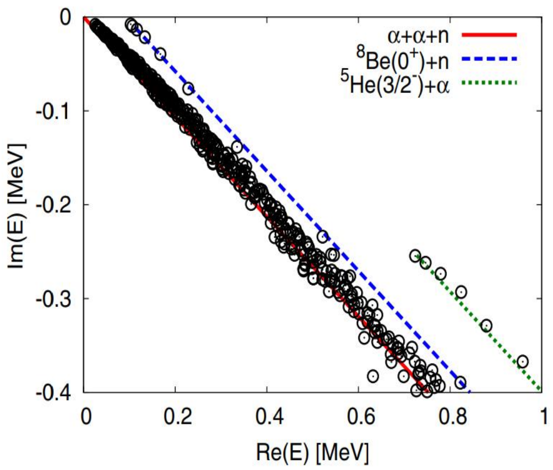

Fig. 2. Distribution of energy eigenvalues of the J$^{\pi}$=1/2^{+} state measured from the α+α+n threshold with scaling angle θ=15 degrees. The three-body potential with $V_3 = -1.02$ MeV and $\mu = 0.02$ fm^{-2} is applied. The solid, dashed, and dotted lines represent the branch cuts for α+α+n, ^{8}Be(0^{+})+n, and ^{5}He($3/2^{-}$)+α continua, respectively.

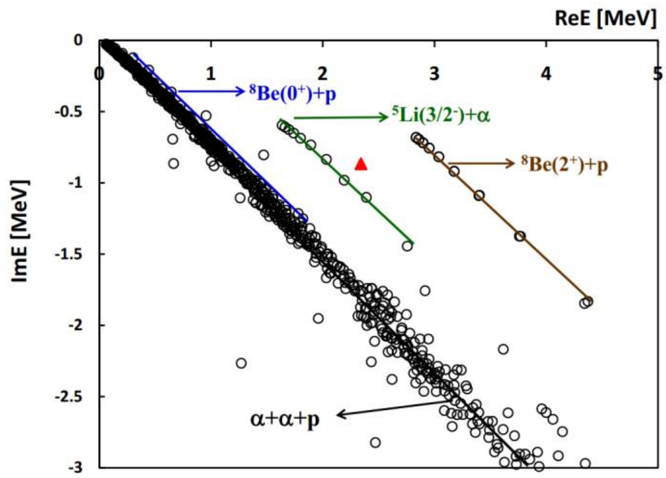

Fig. 3. Distribution of energy eigenvalues of the J$^{\pi}$=1/2^{+} state measured from the α+α+p threshold with scaling angle θ=15 degrees. The three-body potential with $V_3 = -1.02$ MeV and $\mu = 0.02$ fm^{-2} is applied.

4. Conclusion

The first excited states of mirror ^{9}Be and ^{9}B nuclei are studied by using the α+α+N three-body model and the complex scaling method. The first excited state of ^{9}Be is observed in photo-disintegration cross sections showing a sharp peak just above the ^{8}Be(0$^+$)+n threshold. The results indicate that the 1/2$^+$ state of ^{9}Be can be a virtual state consisting of ^{8}Be and valence neutron. Its analog ^{9}B(1/2$^+$) state is further investigated and obtained as the resonance with the resonance energy $E_{res} = 2.42$ MeV with the decay width $\Gamma = 1.61$ MeV.

References

[1] Y. K.Ho, Phys. Rep. **99** (1983) 1.

[2] T. Myo, Y. Kikuchi, H. Masui, K. Katō, Prog. Part. Nucl. Phys. **79** (2014) 1.

[3] M. Odsuren, Y. Kikuchi, T. Myo, M. Aikawa, K. Katō, Phys. Rev. C **92** (2015) 014322.

[4] H. Kanada, T. Kaneko, S. Nagata, and M. Nomoto, Prog. Theor. Phys. **61** (1979) 1327.

[5] C. Kurokawa, K. Kato, Nucl. Phys. A **792** (2007) 87.

[6] D. Tilley et al., Nucl. Phys. A **745** (2004) 155.

[7] H. Utsunomiya, Y. Yonezawa, H. Akimune, T. Yamagata, M. Ohta, M. Fujishiro, H. Toyokawa, H. Ohgaki, Phys. Rev. C **63** (2000) 018801.

[8] C.W. Arnold, T.B. Clegg, C. Iliadis, H.J. Karwowski, G.C. Rich, J.R. Tompkins, C.R. Howell, Phys. Rev. C **85** (2012) 044605.

Refraction Effects in the α and ^{3}He Scattering on Light Nuclei at Energies about 50 MeV

T.K. Zholdybayev[1], N. Burtebayev[1], S.B. Sakuta[2], B. Sadykov[1]

[1] *Institute of Nuclear Physics, 050032 Almaty, Kazakhstan*

[2]*National Research Center "Kurchatov Institute", 123182 Moscow, Russia*

Analysis of scattering data within the optical model is the main source of information about potentials of the nucleus–nucleus interaction. It is well-known, however, that for complex projectiles with $A \geq 2$, such analysis is ambiguous. An especially complicated situation occurs at low energies (E < 10 MeV/nucleon). Numerous studies have shown that the ambiguity in the extracted parameters of the real part of the nuclear potential can be both continuous and discrete.

If the depth of the real part of the nuclear potential is large in comparison with the energy of the incident particle, which is a case at low E/nucleon < 10 MeV energies, then for sufficiently small impact parameters, due to the influence of nuclear attraction, the deflection angle of the scattered particle can exceed 180 degrees. In this case, a diffraction pattern is observed over the entire angular range of the angular distribution. However, at higher energies, the incident particle can be deflected on an angle not exceeding a certain limit. In quantum mechanics, however, the cross section is finite, but at not very strong absorption, a maximum should be observed followed by an exponential decrease at larger angles. This effect appears due to the refractive properties of the real part of the nuclear potential and is analogous to the phenomenon of the rainbow in optics. The magnitude and the angular dependence of the cross sections when the nuclear rainbow is observed are very sensitive to the real part of the nuclear potential as was first shown in papers [1-3]. The analysis of such data using the optical model allows removing a discrete ambiguity in depth of the real part of the nuclear potential. Observation of rainbow in the refraction scattering is very important as it can be used to probe the density dependence of the NN interaction and the nuclear equation of state in the folding model analysis.

The measurements were performed at the isochronous cyclotron U-150M in the Institute of Nuclear Physics (Almaty, Kazakhstan) using extracted beams of ^{3}He and α-particles accelerated to energies of 48.1 MeV (α) and 50, 60 MeV (^{3}He). A gas target was used in the experiment. It was a container of cylindrical shape, filled with natural oxygen (99.76% ^{16}O) and natural nitrogen (99.61% of ^{14}N) to a pressure of about one atmosphere. The effective target thickness was 1–7 mg/cm^2, depending on the angle of measurement. The error in the thickness was not larger than 3%. The construction of the target was described in more detail in [4]. The scattered ^{3}He and α-particles were detected and separated from the other charged reaction products using standard techniques (ΔE–E) with a telescope counters consisting of two silicon detectors with a thickness of 100 microns (ΔE) and 2mm (E). Total energy resolution was about 500 keV and was determined by the energy spread of the beam, the target thickness and the angle of measurement. The uncertainty in our absolute differential cross sections is about 10%.

Differential cross sections for elastic scattering have been measured in the range of angles from 10° to 170° in the laboratory system. Angular distributions, as can be seen from the figures shown in the next section, have a diffractive structure up to angles of 60°–70°. With increasing angle this structure decays and is replaced by a broad maximum with a further fall-off at larger angles without pronounced oscillations.

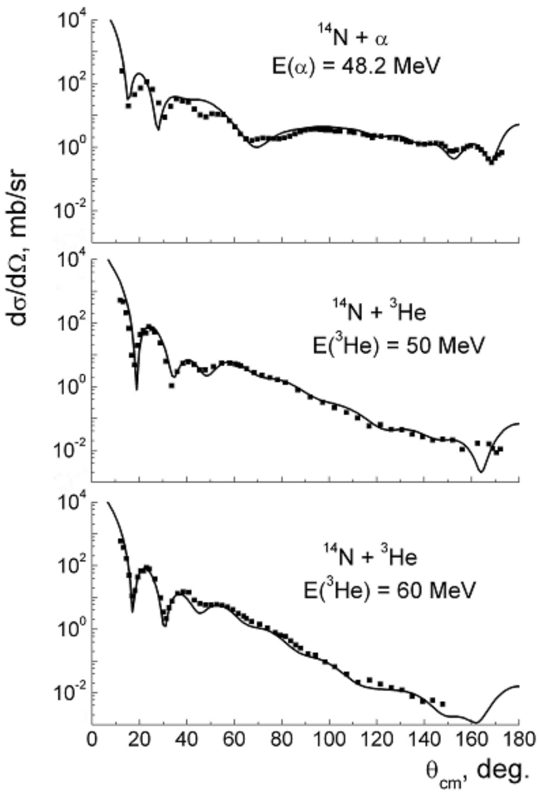

Fig. 2. The angular distributions of the elastic scattering of -particles (E = 48.2 MeV) and ^{3}He at the 50 and 60 MeV energies on ^{14}N nuclei. The points are experimental cross sections. The curves are the optical model calculations.

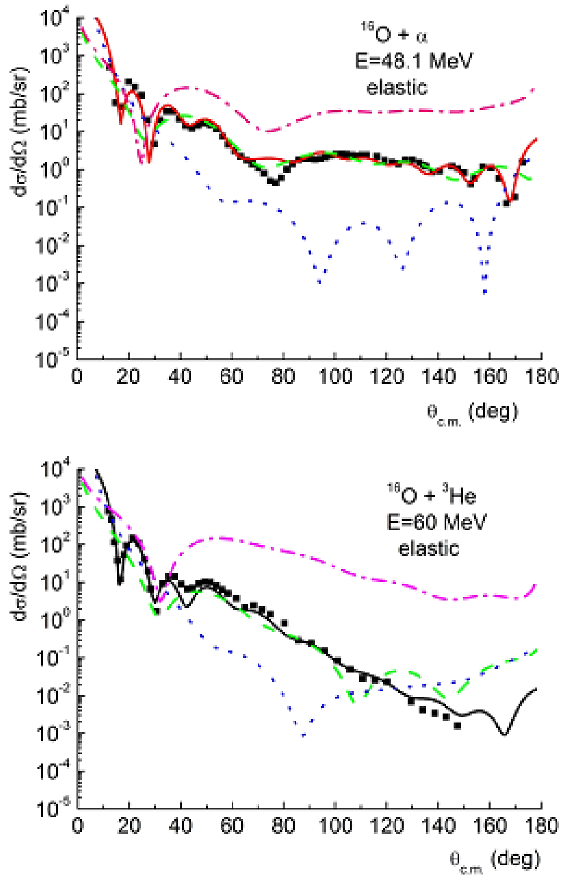

Fig. 3. The elastic scattering of α-particles and ^3He on ^{16}O nuclei. Dots – experiment. Solid curves – the optical model calculations. The dashed and dotted curves show decomposition of the cross sections to the far – and the near – components, respectively. Dot-dashed curves – cross sections for the far component with the zero absorption (W=0).

The experimental data had been analyzed within the framework of the optical model using phenomenological potentials with Woods-Saxon form-factor. The optimal potential parameters were found from the best description of the experimental angular distributions of elastic scattering by the least squares method. As starting potentials, we used potentials which have been found earlier from analysis for scattering of ^3He and α-particles on ^{14}N these nuclei at energies close to ours [5, 6]. To reduce the ambiguity of the search, we tried not to go far from the recommended geometric parameters.

Characteristic features of the measured angular distributions are the well-defined nuclear rainbow effects, manifested in the existence of Airy minima around the angles of 80° (for α-particles) and 40° (for ^{3}He) and the observed unstructured fall-off with increasing scattering angles. The interpretation of these features is more transparent in the quasi-classical approach. In this case, the differential cross section at a given angle is determined by the contributions of the two trajectories. One trajectory corresponds to the scattering at the "near" edge of the nucleus and the other at the "far" edge with amplitudes $f_N(\theta)$ and $f_F(\theta)$, respectively.

Fig. 3 shows the decomposition of the theoretical cross section for elastic scattering into near-side and far-side components. It can be seen that at large angles, the experimental cross sections are almost entirely reproduced by the far-side component $f_F(\theta)$, and at small angles, where the amplitudes $f_N(\theta)$ and $f_F(\theta)$ are comparable, large oscillations are observed due to their interference. The structure of the cross sections for the far-side component occurs due to the interference of the $l>$ and $l<$ trajectories of the deflection function for the scattering at the same angle. It manifests itself more clearly, if one turns off the absorption (W=0). The cross sections calculated with W=0 are shown in **Fig. 3** by the dot–dashed curves. It is evident that in ^{3}He scattering, only one minimum at the angle about 30° is observed, while for α-particles, there are two minima (at ~80° and ~30°) associated with the manifestation of the primary and secondary nuclear rainbows. Thus, in the elastic scattering of α-particles and ^{3}He on ^{16}O energies near 50 MeV, with the same momentum transfers, nuclear rainbow effects are well pronounced due to the refractive properties of the two nuclear potentials.

References

[1] D.A. Goldberg, S.M. Smith, Phys. Rev. Lett. **29** (1972) 500.

[2] D.A. Goldberg, S.M. Smith, G.E. Burdzik, Phys. Rev. C **10** (1974) 1362.

[3] D.T. Khoa, W. von Oertzen, H.G. Bohlen, S. Ohkudo, J. Phys. G: Nucl. Part. Phys. **34** (2007) 111.

[4] A.D. Duisebayev et al., Izv. KazSSR AN. Ser. Fiz.-Mat. **4** (1984) 73.

[5] G.R. Satchler, W.G. Love, Phys. Rep. **55** (1979) 183.

[6] N. Burtebayev et al., Acta. Phys. Pol. **47** (2016) 2017.

Analysis of the ^{16}O(p,pn)^{15}O Reaction Using the CDCC Method

D. Ichinkhorloo[1], M. Aikawa[2], S. Chiba[3,4], Y. Hirabayashi[5], and K. Katō[1]

[1]*Nuclear Reaction Data Centre, Faculty of Science, Hokkaido University, Sapporo 060-0810, Japan*

[2]*Faculty of Science, Hokkaido University, Sapporo 060-0810, Japan*

[3]*Research Laboratory for Nuclear Reactors, Tokyo Institute of Technology, Tokyo 152-8550, Japan*

[4]*National Astronomical Observatory of Japan, Mitaka, Tokyo 181-8588, Japan*

[5]*Information Initiative Center, Hokkaido University, Sapporo 060-0811, Japan*

The study of the ^{16}O(p,pn)^{15}O reaction is valuable in the nuclear reaction data field and applicable to on-line PET (positron emission therapy) in the medical field. However, the experimental data show a discrepancy and a reliable theoretical calculation is desired.

The continuum-discretized coupled-channel (CDCC) method is a promising approach for nuclear reactions involving light nuclei with a cluster structure. In the previous works [1-4], we have successfully studied reaction data for the ^{6,7}Li + n elastic and inelastic scattering angular distributions and neutron spectra applying the CDCC method [5] with $\alpha + d + n$ and $\alpha + t + n$ models.

In this work, we applied the CDCC analysis to the different target of ^{16}O with the incident proton energies up to 70 MeV. We calculate the reaction cross sections of ^{16}O(p,pn)^{15}O using ^{15}O + n + p models with the CDCC method. Comparing the results of calculations with experimental data, we discuss reaction data for ^{16}O(p,pn)^{15}O with the present CDCC calculations using the cluster folding potential of the optical model potential (OMP).

The three-body system shown in **Fig. 1** is described by a model Hamiltonian

$$H = H_{^{15}O-n} + K_R + U,$$

$$H_{^{15}O-n} = K_r + V_{^{15}O-n}\left(r\right),$$

$$U = U_{n,p}\left(r_{n,p}\right) + U_{^{15}O,p}\left(r_{^{15}O,p}\right). \quad (1)$$

Vector $\vec{r}$ is the relative coordinate between *n* and ^{15}O, $\vec{R}$ the one between the center of mass of the *n*-^{15}O pair and *p*, and $\vec{r}_{n,p}\left(\vec{r}_{^{16}O,n}\right)$ denotes the relative coordinate between two particles *n* (^{15}O) and *p*. Operators K_r and K_R are kinetic energies associated with $\vec{r}$ and $\vec{R}$, respectively, and $V_{^{15}O,n}\left(\vec{r}\right)$ is the interaction between *n* and ^{15}O. The interaction $U_{n,p}$ ($U_{^{15}O,p}$) between *n* (^{15}O) and *p* is taken to be the optical potential for *n*+*p* (^{15}O+*p*) scattering (**Table 1**). We prepare the wave functions of the bound and ^{15}O+*n* scattering states of ^{16}O in the similar way as previous works [1-3] in the CDCC method.

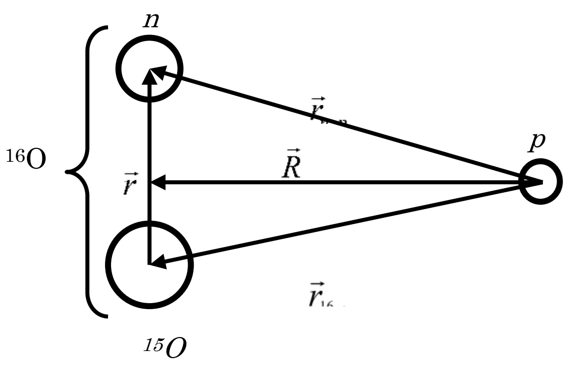

Fig. 1. Illustration of the ^{15}O+*n*+*p* three-body system.

Table 1. Parameters of the optical potentials for *n*+*p* and ^{15}O+*p*.

System	V_0	r_0(fm)	a_0(fm)	W_0(MeV)	r_W(fm)	a_W(fm)	W_D(MeV)	r_{WD}(fm)	a_{WD}(fm)
$n+p$ [6]	92.1	1.05	0.500	-	-	-	7.67	1.02	0.511
^{15}O + p [7]	43.9	1.13	0.660	4.54	1.42	0.48	2.93	1.42	0.480

Using the current method, we analyze the elastic scattering cross sections and breakup cross section of the ^{16}O+*p* collision at incident proton energies up to 70 MeV. We take three normalization factors, λ_V for all channels in the real part, $\lambda_{w.el}$ for the ground-ground channel and $\lambda_{w.BU}$ for the other channels in the imaginary part. The factors λ_V and $\lambda_{w.el}$ are set to be 1.0 to reproduce elastic angular distributions. The factor $\lambda_{w.BU}$ has a very small contribution to the elastic angular distribution, although a large contribution to the breakup channels. The last one is used as a free parameter and set to be 0.1 in the following discussion.

Fig. 2 shows the angular distribution of the ^{16}O + p elastic scattering with incident energies between 35 and 65MeV. The results of the CDCC calculation represented with solid lines are in good agreement with the experimental data. In **Fig. 3**, the breakup cross-sections for the ^{16}O(p,pn)^{15}O reaction are shown with the experimental data [12-15]. The calculated result underestimates the experimental data, however the behaviour is almost consistent. One of the reasons for the discrepancy is the selection of the factor $\lambda_{\mathrm{w.BU}}$. The best parameter of the factor $\lambda_{\mathrm{w.BU}}$ will be searched.

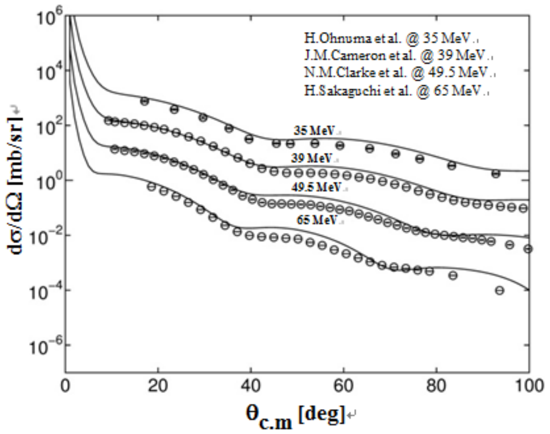

Fig. 2. Elastic angular distribution of ^{16}O+p scattering.

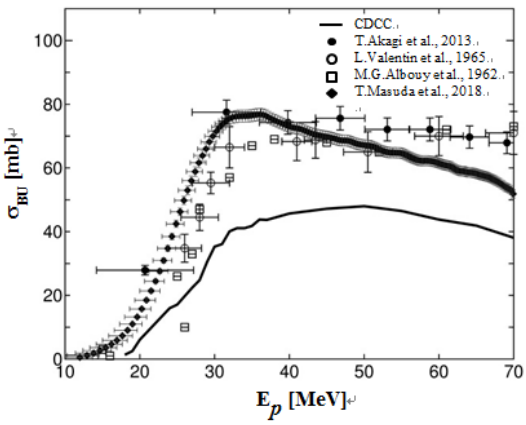

Fig. 3. Breakup cross section of ^{16}O(p,pn)^{15}O reaction.

In the summary, applying the CDCC framework to the ^{15}O + n + p model, we investigated the proton elastic angular distribution and breakup cross sections for the ^{16}O targets, respectively, at incident proton energies up to 70 MeV. The CDCC calculation gives a satisfactory good agreement with the experimental data. Although our model calculation is still short of the strength of breakup cross sections. This may suggest that our model is too simple. It is desirable to include other degrees of freedom in ^{16}O and to extend the CDCC method in the next study.

References

[1] T. Matsumoto, D.Ichinkhorloo, Y.Hirabayashi, K.Katō, and S.Chiba, Phys. Rev. C **83** (2011) 064611.

[2] D.Ichinkhorloo, T.Matsumoto, Y.Hirabayashi, K.Katō and S.Chiba, J. Nucl. Sci. Technol. **48** (2011) 1357.

[3] D.Ichinkhorloo, Y.Hirabayashi, K.Katō, M. Aikawa, T.Matsumoto, and S.Chiba, Phys. Rev. C **83** (2012) 064604.

[4] D.Ichinkhorloo, M.Aikawa, S.Chiba, Y.Hirabayashi and K.Kato, Low energy scattering cross sections for n +6,7Li reactions using the continuum-discretized coupled-channels method, Phys. Rev. C **93** (2016) 064612.
[5] M.Kamimura, M.Yahiro, Y.Iseri, Y.Sakuragi, H.Kameyama and M.Kawai, Prog. Theor. Phys. Suppl. No. 89 (1986).
[6] P.Hinterberger et al., Nucl. Phys. A **111** (1968) 265.
[7] J.L.Shelgrove and E.Kashy, Phys. Rev. **187** (1969) 1259.
[8] H.Ohnuma et al., Nucl. Phys. A **514** (1990).
[9] J.M.Cameron et al., Phys. Rev. **167** (1969) 908.
[10] N.M.Clarke et al., Nucl. Phys. A **157** (1970) 145.
[11] H.Sakaguchi et al., Phys. Rev. C **26** (1982) 944.
[12] T.Masuda et al., Scientific Reports **8** (2018) 2570.
[13] T.Akagi et al., Radiation Measurements **59** (2013) 262.
[14] M.Sajjad et al., RCA **38** (1985) 57.
[15] M.G.Albouy et al., PL **2** (1962) 306.

Development of a Semi-empirical Model for Calculation of Fission Product Yields

Jounghwa Lee[1,2], Choong-Sup Gil[1], Young-Ouk Lee[1], Tae-Sun Park[2], Seung-Woo Hong[2]

[1]*Nuclear Data Center, Korea Atomic Energy Research Institute, Daejeon 34057, Korea*

[2]*Department of Physics, Sungkyunkwan University, Suwon 16419, Korea*

Numerous attempts were made in the past to describe the fission process since fission was discovered, but our understanding about fission is still far from being complete. Fission product yield data are important for applications of nuclear technology such as the estimation of decay heat, operation of nuclear reactors and so on. However, it is hard to obtain fission product yields from measurements because of their short live-times. Therefore, fission models are required to calculate fission product yields of nuclides that have no or poorly measured yield data. Even though theoretical fission models improved our understanding of nuclear fission process, the calculation results are not necessarily accurate enough to reproduce the fission observables quantitatively. On the other hand, semi-empirical models reproduce experimental data with a relatively good accuracy. Therefore, we developed a model for fission product yields in neutron-induced fissions of actinides for thermal and fast (500 keV) neutrons using semi-empirical method.

We describe the fission product yields of actinides (uranium and plutonium) by assuming that fission product yields are proportional to the level density of the microcanonical ensemble of the compound nucleus at the fission barrier. The fission height, the energy of compound nucleus required for the deformation is modeled as a sum of symmetric and asymmetric part. They are expressed by parabolic and Gaussian functions, respectively. The detail of the model is described in ref. [1]. It should be mentioned that we use the values of $\gamma = 0.1\ \mathrm{MeV}^{-1}$ for uranium isotopes and $0.11\ \mathrm{MeV}^{-1}$ for plutonium isotopes rather than adopt the values of $\gamma = 0.06\ \mathrm{MeV}^{-1}$ which is determined by a statistical analysis of level density data [2]. This is because we found that our model reproduce the valley region of mass distribution batter when we adjust the damping parameter γ. We set $V_0 = 5\ \mathrm{MeV}$ and $N_{in} = 82$ in common for both uranium and plutonium isotopes. For C_{mac}, we adopt the value given in ref. [3]. For rest parameters ($C_{in}, C_{out}, N_{out}, \sigma_{in}, \sigma_{out}$ and $\tilde{a}$), the fitting method expressed in ref. [1] is used. **Table 1** shows our ten model parameters for uranium and plutonium isotopes, which are used for the calculation of mass distribution.

Table 1 The model parameters for uranium and plutonium isotopes.

	U	Pu
N_{out}	89.98	90.37
C_{in} (MeV)	-4.48	-4.94
C_{out} (MeV)	-9.39	-9.95
$\tilde{a}$ (MeV^{-1})	-5.23A_{CN}+1262	-1.74A_{CN}+440
σ_{in}	-0.50A_{CN}+124	-0.36A_{CN}+92.5
σ_{out}	4.93	5.13
γ	0.1	0.11
V_0 (MeV)	5	
N_{in}	82	
C_{mac}	$\left(\frac{8}{N_{CN}^2}\right)10^{7.16993-0.26602\left(\frac{Z_{CN}^2}{A_{CN}}\right)+0.00283\left(\frac{Z_{CN}^2}{A_{CN}}\right)^2}$	

We calculated the mass distribution of fission products using the parameters given in the table 1. A part of our calculation is shown in **Fig. 1**. The calculation results from other phenomenological fission models, TALYS and GEF, are also expressed in **Fig. 1** as well as the experimental data from EXFOR and ENDF/B-VII.1 data. As can be seen in **Fig. 1**, the overall shape of mass distributions are reproduced quite well using our model while the valley region and the far sides of wing are not reproduced well. In addition, our model should be improved to describe the detailed structures near the peaks.

Except $\tilde{a}$ and σ_{in}, our model parameters that used to calculate the mass distribution of uranium isotopes are the same or similar with those of plutonium (**Table 1**). Therefore, we expect to find the global parameters that can be used to calculate the fission product mass distribution of all fissioning nuclei.

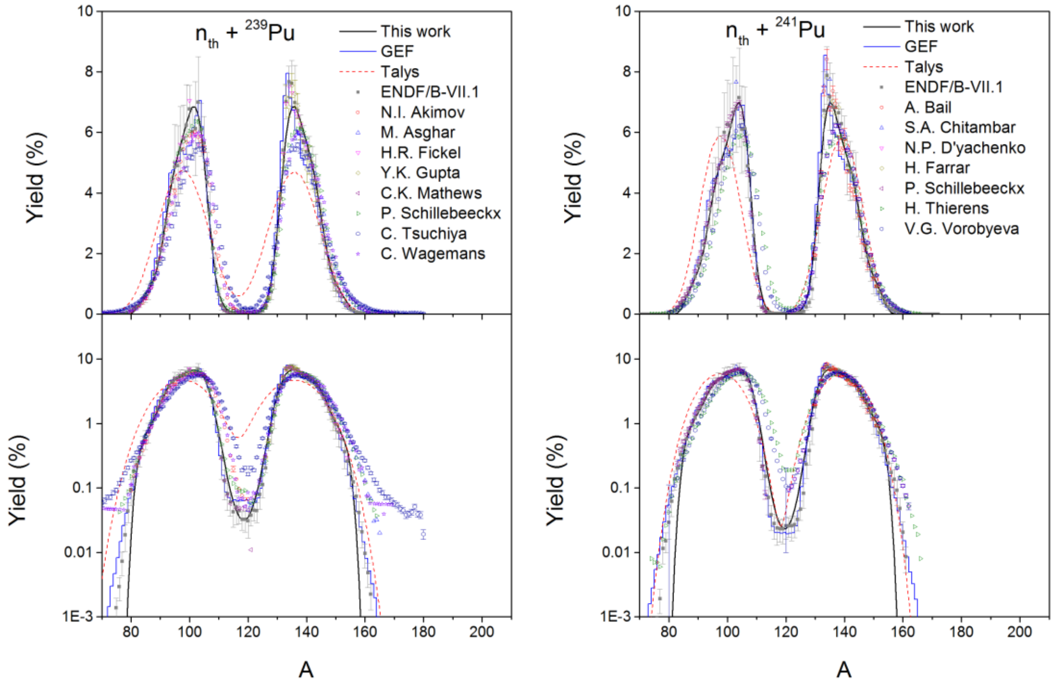

Fig. 1. For thermal neutron induced fission of ^{239}Pu(left) and ^{241}Pu(right), our results for fission product yields that plotted by the black full line are compared with the experimental data, ENDF/B-VII.1, and the results from GEF, the blue step line, and TALYS, the red dashed line. The same results are plotted in linear and logarithmic scales, respectively, in the upper and lower panels.

References

[1] J. Lee, C.-S. Gil, Y.-O. Lee, T.-S. Park, S.-W. Hong, Eur. Phys. J. A **54** (2018) 173.

[2] T. von Egidy, D. Bucurescu, Phys. Rev. C **72** (2005) 044311.

[3] J. Benlliure, A. Grewe, M. de Jong, K.-H. Schmidt, S. Zhdanov, Nucl. Phys. A **628** (1998) 458.

Systematic Study on Charged-particle-induced Reactions for Medical Radioisotope Production

M. Aikawa[1], M. Saito[2], T. Murata[2], M. Sakaguchi[3]

[1]*Faculty of Science, Hokkaido University, Sapporo 060-0810, Japan*
[2]*Graduate School of Biomedical Science and Engineering, Hokkaido University, Sapporo 060-8638, Japan*
[3]*School of Science, Hokkaido University, Sapporo 060-0810, Japan*

Radioisotopes are available for nuclear medicine, e.g. diagnosis and therapy. In order to produce the radioisotopes from stable nuclides, nuclear reactions using nuclear reactors and accelerators are required. There are basically several reactions to produce each radioisotope. Investigations of such reactions are necessary to find reactions with less byproducts and with higher cost effectiveness.

One of reaction types is charged-particle-induced reactions. The reactions have an advantage to change atomic numbers from those of targets and to chemically separate the products from the targets.

There are many charged-particle-induced reactions to be investigated for nuclear medicine. We therefore continuously study the reactions to obtain fundamental information of nuclear data and to select the best reaction among possible reactions. The systematic study is conducted under the collaboration with researchers in RIKEN, Japan and ATOMKI, Hungary. In this paper, we report current status of our experiments performed in 2018 and one of the results, the excitation function of the deuteron-induced reaction on ^{93}Nb for production of a medical RI candidate, ^{93m}Mo ($T_{1/2}$ = 6.85 d) [1].

We adopted standard methods, stacked foil activation method and high-resolution gamma-ray spectrometry, to determine cross sections. Experiments were performed at the AVF cyclotron of the RIKEN RI Beam Factory. The facility produces deuteron and alpha beams up to 24 and 50 MeV. Several targets stacked with elementally pure metallic foils were irradiated by the beams. The experiments which we have performed in 2018 are listed in **Table 1**.

The excitation function of the ^{93}Nb(d,x)^{93m}Mo reaction up to 24 MeV was derived from the γ-line at 263.049 keV (I_γ =57.4%) from the ^{93m}Mo IT decay. The measurement was performed after a cooling time of about 10 hours for background reduction. The result is shown in **Fig. 1** in comparison with the literature data [2-4] and the TENDL-2017 data [5]. Our result is in good agreement with the other experimental data. The TENDL-2017 data overestimates all the experimental data including ours.

Table 1. Experiments performed in 2018.

Target	Beam	Beam time	Status
^{nat}Ag	α	Mar. 2018	Published [6]
^{nat}Ni	α	Mar. 2018	Analyzing
^{89}Y	α	Mar. 2018	Analyzing
^{93}Nb	d	Jun. 2018	Published [7]
^{89}Y	d	Sep. 2018	Analyzing
^{nat}Er	α	Sep. 2018	Analyzing

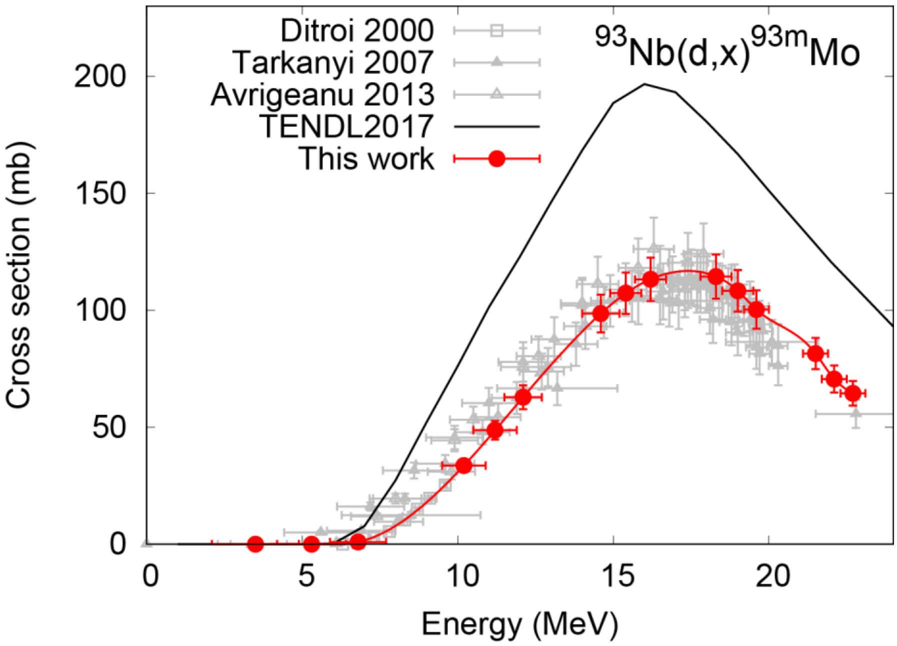

Fig. 1. The excitation function of the ^{93}Nb(d,2n)^{93m}Mo reaction.

In summary, we systematically study nuclear reactions for medical RI production to select reactions with less by products and with higher cost effectiveness. The status of experiments which we have performed in 2018 and the excitation function of the ^{93}Nb(d,x)^{93m}Mo reaction as an example were reported.

This work was carried out at RI Beam Factory operated by RIKEN Nishina Center and CNS, University of Tokyo, Japan. This work was supported by JSPS KAKENHI Grant Number 17K07004. The authors are particularly grateful to S. Takács and F. Ditrói (ATOMKI) and Y. Komori and H. Haba (RIKEN).

Reference

[1] M. Sadeghi, M. Enferadi, H. Nadi, C. Tenreiro, A novel method for the cyclotron production no-carrier-added ^{93m}Mo for nuclear medicine, J. Radioanal. Nucl. Chem. **286** (2010) 141.

[2] F. Ditrói, F. Tárkányi, M.A. Ali, Investigation of deuteron induced nuclear reactions on niobium, Nucl. Instr. Meth. B. **161–163** (2000) 172.

[3] F. Tárkányi, A. Hermanne, F. Ditrói, S. Takács, B. Király, M. Baba, T. Ohtsuki, S.F. Kovalev, A. V. Ignatyuk, Production of longer lived radionuclides in deuteron induced reactions on niobium, Nucl. Instr. Meth. B **255** (2007) 297.

[4] M. Avrigeanu, V. Avrigeanu, P. Bém, U. Fischer, M. Honusek, A.J. Koning, J. Mrázek, E. Šimečková, M. Štefánik, L. Závorka, Low-energy deuteron-induced reactions on ^{93}Nb, Phys. Rev. C **88** (2013) 014612.

[5] A.J. Koning, D. Rochman, Modern Nuclear Data Evaluation with the TALYS Code System, Nucl. Data Sheets **113** (2012) 2841.

[6] F. Ditrói, S. Takács, H. Haba, Y. Komori, M. Aikawa, M. Saito, T. Murata, Investigation of alpha particle induced reactions on natural silver in the 40-50 MeV energy range, Nucl. Instr. Meth. B **436** (2018) 119.

[7] M. Aikawa, Y. Komori, H. Haba, Activation cross sections of deuteron-induced reactions on niobium up to 24 MeV, Nucl. Instr. Meth. B **436** (2018) 217.

Proton Induced Reaction Cross Sections of ^{nat}W with Proton Beam of 45 MeV

Nguyen Thi Hien[1], Guinyun Kim[1], , Kwangsoo Kim[1], Nguyen Van Do[2,3], Nguyen Thanh Luan[3]

[1]*Department of Physics, Kyungpook National University, Daegu 702-701, Korea*

[2]*Institute of Fundamental Research and Application, Duy Tan University, 73 Hoang Cau Street, Hanoi, Vietnam*

[3]*Institute of Physics, Vietnam Academy of Science and Technology, 10 Dao Tan, Hanoi, Vietnam*

In this work, the production cross sections for the $^{nat}W(p,x)^{182m,g;184m,g}Re$ reactions within the energy range from their threshold up to around 45 MeV have been determined using the stacked- foil activation and off-line γ-ray spectrometric technique at the MC50 cyclotron of the Korea Institute of Radiological and Medical Sciences (KIRAMS). The proton energy for each foil in the stacked-foils was calculated by using the SRIM-2003 program. The natural copper (^{nat}Cu) foils were used as monitor foils to determine the proton beam flux to determine the cross-sections for the $^{nat}W(p,x)$ reactions. The experimental results from the present work were compared with the literature data and theoretical values from TENDL-2015 database library.

Keywords: $^{nat}W(p,x)$ reaction cross sections, stacked- foil activation technique, off-line γ-ray spectrometric technique, MC50 cyclotron, TENDL-2015.

Measurements of Cross Section for the Theranostic Radionuclide ^{67}Cu

J. K. Park[1], M.-H. Jung[1], Y. S. Hwang[1], C. Kim[1], W.-J. Cho[1], and S.-C. Yang[2]

[1]*Korea Multi-purpose Accelerator Complex (KOMAC), Korea Atomic Energy Research Institute (KAERI), Gyeongju 38180, Korea*

[2]*Nuclear Data Center, Korea Atomic Energy Research Institute (KAERI), Daejeon 34057, Korea*

E-mail: jkuepark@kaeri.re.kr

One of the major theranostic isotopes, ^{67}Cu, has the specific role of copper in several biochemical processes and is an excellent nuclide for radioimmuno-therapy owing to its peculiar physical-chemical characteristics. Here, we thus present the cross sections for the ^{nat}Zn(p,x)^{67}Cu and ^{nat}Zn(p,x)^{67}Ga reactions within a proton energy range of 47 to 99 MeV. For overlapping gamma-ray spectra of the two isotopes of ^{67}Cu and ^{67}Ga, we efficiently separated them by employing an analytical method without supporting a radiochemical separation. The present data are compared with the previous literature data, which were typically obtained by radiochemical separation before measuring the gamma-ray spectra of the two isotopes. Our results for two isotopes show in general, greater or smaller values than the literature data except for some data in a partial energy range that are in agreement with the literature data. The present data are also compared with the TENDL-2017 library based on the TALYS code.

Keywords: cross-section, proton beam, ^{nat}Zn(p,x)^{67}Cu, ^{nat}Zn(p,x)^{67}Ga

Visualization of Fission Product Yield by NDPlot

Yongli Jin[1], Nengchuan Shu[1], Xi Tao[1], Jimin Wang[1], Jing Qian[1] , Zhigang Ge[1]

[1]*China Nuclear Data Center, P.O.BOX 275-41,Beijing,China*

NDPlot is an efficient plotting tool for nuclear data, and also is an integrated application software. The system includes database, application service and client software. There are three properties in NDPlot:

Convenience: It has a friendly human-machine interface.

Traceability: Information can be stored in a project file, including the original data, coordinate system, annotations and memos etc. The users can read it at any time.

Reusability: Users can save or continue their work whenever necessary. The project file can be used for continuing or checking the work by others.

Architecture of NDPlot is Client-Server structure. The original ENDF and EXFOR libraries are stored in database, retrieved and handled by the application service. The plotting data are handled by NDPlot client, which is developed with Perl language, and its GUI platform is WxWindows. The multi-document interface (MDI) is used in NDPlot, more than one window are displayed simultaneously (**Fig. 1**). The batch plotting function can be used to plot more than one reactions in a window, and a factor (such as 0.01) can be defined to separate the reactions (**Fig. 2**).

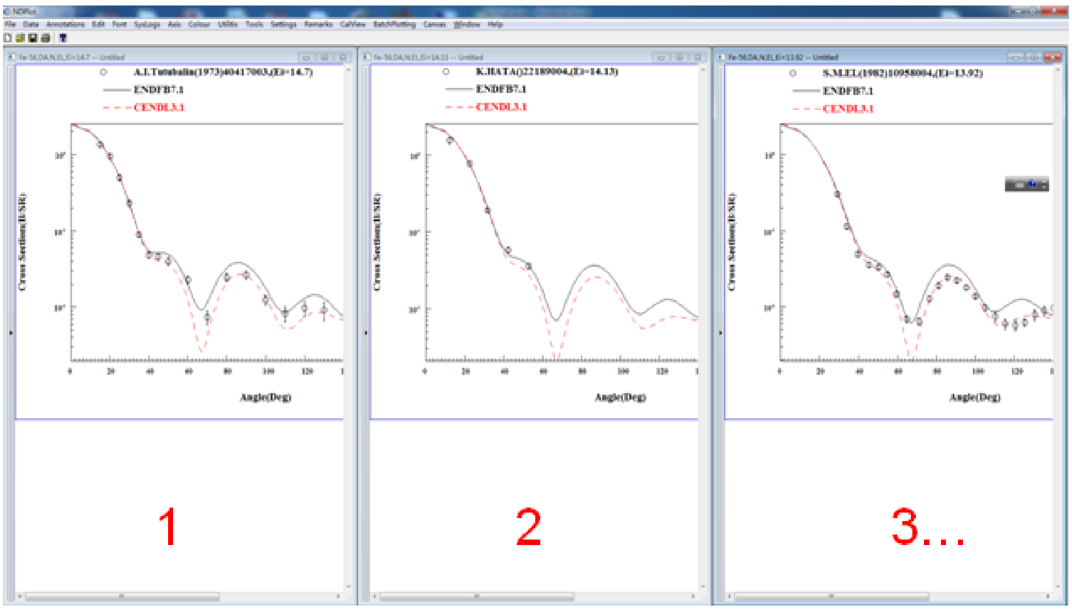

Fig. 1. Screenshot of NDPlot.

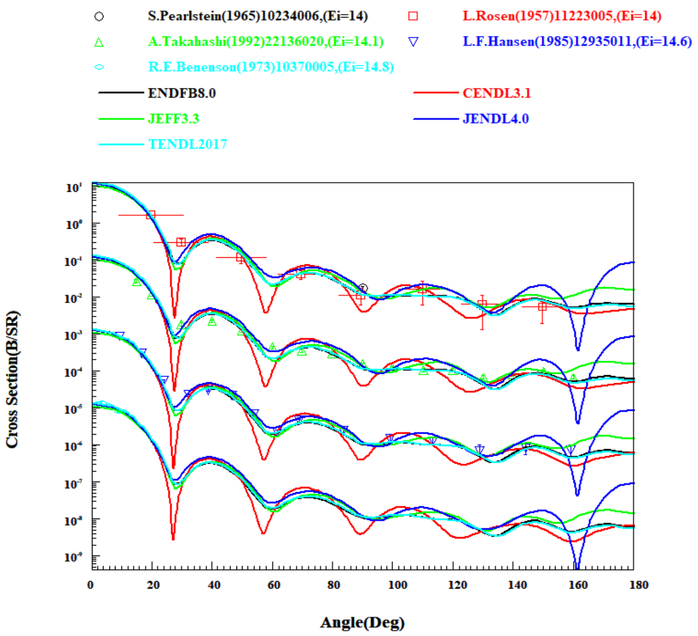

Fig. 2. Batch Plotting with factor 0.01(Ta-181(n, el),DA).

Since the end of 2016, we devoted ourselves to development of NDPlot. Now, NDPlot can plot experimental and evaluated data of nuclear reaction cross sections, angular distributions of secondary particles, energy distributions of secondary particles, energy-angle distributions of products, number of neutrons per fission and ratio of cross sections (**Fig. 3**) and so on.

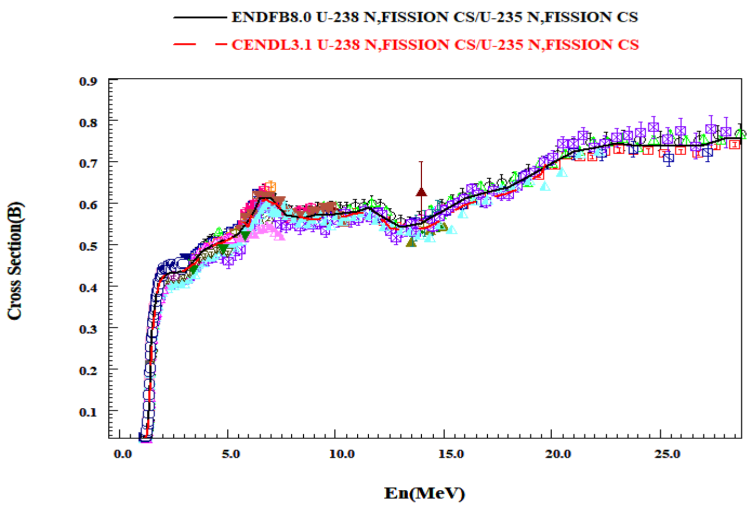

Fig. 3. Ratio of nuclear reaction cross sections.

Since September 2018, NDPlot has been able to plot the chain yields and energy dependent fission product yields, including experimental data and evaluated data (**Fig. 4** and **Fig. 5**). NDPlot also provides tools to filter fission yield data and correct the data with new gamma data. The decay data and flag data in EXFOR are used to correct or distinguish the experimental data, in addition there are more complex structures for the experimental data of fission product yield (FPY). So a variable length column as information column was added, which can store decay data, flag data and fission product yield.

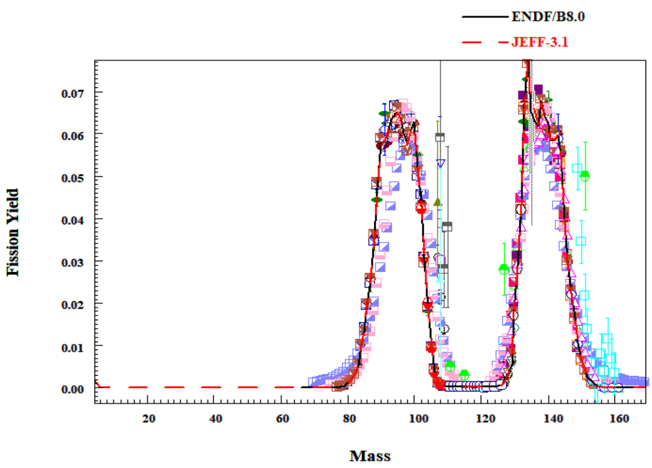

Fig.4. Chain Yield of U-235 (Thermal Energy).

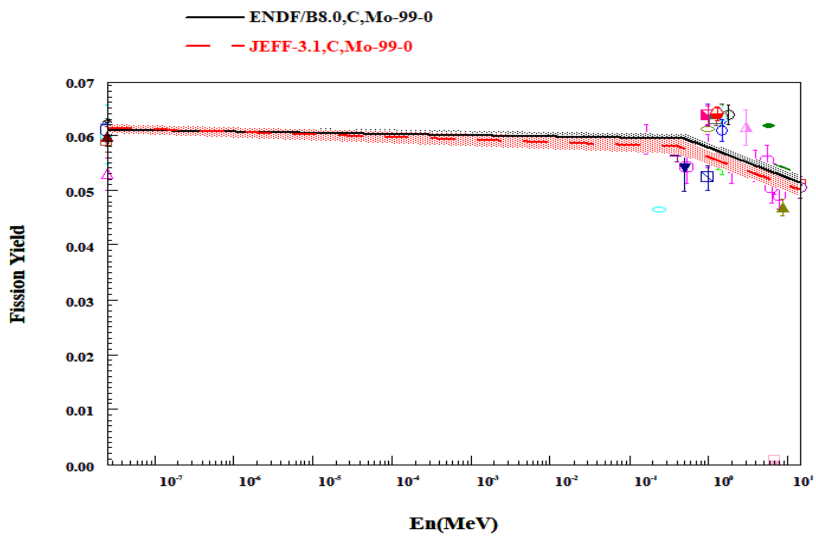

Fig.5. Energy Dependent Fission Product Yields.

(U-235 (N,F)42-Mo-99,CUM,FY)

In the latest version, NDPlot 0.92 beta, for the requirements of evaluator on discrete level excitation cross sections, a special treatment was added which will help user to determine which MT number will be chosen in the pop-up window.

	Choice	ENDFB8.0	Choice	CENDL3.1
7	☐	3.122970Mev : MT=57	☐	3.122927Mev : MT=57
8	☐	3.369950Mev : MT=58	☐	3.369840Mev : MT=58
9	☐	3.388550Mev : MT=59	☐	3.388550Mev : MT=59
10	☐	3.445349Mev : MT=60	☐	3.445306Mev : MT=60
11	☐	3.448411Mev : MT=61	☐	3.448410Mev : MT=61
12	☐	3.600210Mev : MT=62	☐	3.602100Mev : MT=62
13	☐	3.605690Mev : MT=63	☐	3.744130Mev : MT=63
14	☐	3.610210Mev : MT=64	☐	3.755570Mev : MT=64
15	☐	3.744130Mev : MT=65	☐	3.829770Mev : MT=65
16	☐	3.755570Mev : MT=66	☐	3.856449Mev : MT=66
17	☐	3.759600Mev : MT=67	☐	4.048826Mev : MT=67
18	☐	3.829770Mev : MT=68	☐	4.100307Mev : MT=68
19	☐	3.856495Mev : MT=69	☐	4.119870Mev : MT=69
20	☐	4.048889Mev : MT=70	☐	4.298039Mev : MT=70

Fig. 6. Choosing levels.

NDPlot code can be downloaded from Website http://www.nuclear.csdb.cn/ndplot/. New functions will be developed in future.

References

[1] <<Programming Perl>> Larry Wall,O'REILLY.

[2] Web site: http://www-nds.iaea.org.

[3] Web site: http://www.wxwidgets.org.

[4] Web site: https://www-nds.iaea.org/public/endf/prepro/.

[5] Web site: https://www-nds.iaea.org/public/endf/endver/.

[6] Web site: http://www.nuclear.csdb.cn/ndplot/.

List of participants

No.	Name	Affiliation	E-mail
1	Naohiko Otsuka	IAEA	N.Otsuka@iaea.org
2	Timur Zholdybayev	INP, Kazakhstan	zholdybayev@inp.kz
3	Ichinkhorloo Dagvadorj	JCPRG, Japan	ichinkhorloo@nucl.sci.ac.jp
4	Myagmarjav Odsuren	NUM, Mongolia	odsuren@seas.num.edu.mn
5	Vidya Devi	IET, Bhaddal, India	vidyathakur@yahoo.co.in
6	Jin Yongli	CIAE, China	jyl@ciae.ac.cn
7	Jimin Wang	CIAE, China	jmwang@ciae.ac.cn
8	Sung-Chul Yang	KAERI, Korea	scyang@kaeri.re.kr
9	Kil-Byoung Chai	KAERI, Korea	kbchai@kaeri.re.kr
10	Sejin Lee	KAERI, Korea	leesj@kaeri.re.kr
11	Haelee Hyun	KAERI, Korea	hyunhl@kaeri.re.kr
12	Choong-Sup Gil	KAERI, Korea	csgil@kaeri.re.kr
13	Jong Woon Kim	KAERI, Korea	jwkim@kaeri.re.kr
14	Young-Sik Cho	KAERI, Korea	yscho@kaeri.re.kr
15	Jounghwa Lee	KAERI, Korea	leejh033@kaeri.re.kr
16	Nguyen Van Do	VAST, Vietnam	ngvando@iop.vast.ac.vn
17	Haradhara Naik	KNU, Daegu, Korea	naikbarc@yahoo.com
18	Nguyen Thanh Luan	VAST, Vietnam	ntluan@iop.vast.ac.vn
19	Nguyen Thi Hien	KNU, Daegu, Korea	nthien@iop.vast.ac.vn
20	Manwoo Lee	DIRAMS, Korea	manura90@gmail.com
21	Tae-Young Song	KAERI, Korea	tysong@kaeri.re.kr
22	Young-Ouk Lee	KAERI, Korea	yolee@kaeri.re.kr
23	Guinyun Kim	KNU, Daegu, Korea	gnkim@knu.ac.kr
24	Seung-Woo Hong	SKKU, Korea	swhong@skku.ac.kr
25	JunKue Park	KAERI, Korea	jkuepark@kaeri.re.kr
26	MyungHwan Mun	KISTI, Korea	aa3103@gmail.com
27	Masayuki Aikawa	Hokkaido Univ., Japan	aikawa@sci.hokudai.ac.jp
28	Taesun Park	SKKU, Korea	taesunpark@skku.edu
29	Duck-Hee Kwon	KAERI, Korea	hkwon@kaeri.re.kr
30	Tae-Ik Ro	DAU, Busan, Korea	tiro@donga.ac.kr

Nuclear Data Section
International Atomic Energy Agency
P.O. Box 100
A-1400 Vienna
Austria

E-mail: nds.contact-point@iaea.org
Fax: (43-1) 26007
Telephone: (43-1) 2600 21725
Web: http://www-nds.iaea.org/